

Smearred Modeling of Hydraulic Fracture Using Partially Coupled Reservoir and Geomechanics Simulators

Morteza Roostaei, Siavash Taghipoor, Alireza Nouri, Vahidoddin Fattahpour, Dave Chan
Department of Civil and Environmental Engineering, University of Alberta

Abstract

There are aspects of the hydraulic fracturing process that remain unresolved for weakly consolidated sandstones. These issues include fracture modes and geometries for weak sandstones, and higher-than-expected fracture pressure in some field projects. The development of shear bands and the concomitant shear dilation may result in stress alterations in the reservoir, requiring higher injection pressures to induce tensile fractures. Further, pressure redistribution in the medium can result in stress increases, hence, create conditions in which a tensile fracture may not be induced under operating conditions.

In this paper, a smeared fracture type hydraulic fracture simulator is developed through numerical coupling between an in-house reservoir simulator and a geomechanical commercial software (FLAC2D). The new package falls within the category of partially decoupled model and is versatile, flexible and efficient. This approach can be used to couple any other advanced commercial fluid flow or geomechanical simulators for an accurate description of the initiation and propagation of hydraulic fractures.

The paper contains a discussion of the partial coupling technique to link fluid flow and geomechanical calculations in modeling fracture initiation and propagation. The models use a common gridblock for the fracture and reservoir and use the deformation calculations to update the porosity and permeability. The method captures the interactive effects of the fracture on reservoir fluid flow and formation geomechanics through stress dependent permeability and porosity.

The developed smeared fracture model can capture both tensile and shear fractures in the formation. Major features of this model include modeling poroelasticity and plasticity, matrix flow, shear and tensile fracturing with concomitant permeability enhancement, saturation-dependent permeability, stress-dependent stiffness and gradual degradation of oil sands due to dilatant shear deformation. The model has been applied to numerically simulate field size hydraulic fracturing in oil sands during cold water injection to show the predictive capability of the simulator.

Keywords: Hydraulic fracturing, Smear fracture; Numerical simulation

1. Introduction

Existing numerical hydraulic fracture models are based either on smeared fracturing (Chin and Montgomery, 2004; Zhai and Sharma, 2005; Zhai, 2006; Xu, 2010; Xu and Wong, 2010; Xu et al., 2010), or discrete fracture (Hagoort et al., 1980; Settari, 1980; Nghiem et al., 1984; Settari, 1988; Settari et al., 1989; Settari et al., 1990; Settari et al., 1992; Papanastasiou, 1997a; Papanastasiou, 1997b; Papanastasiou, 1999; van Dam et al., 2000; Settari et al., 2002a; Settari et al., 2002b; Ji et al., 2004; Ji et al., 2006; Wu, 2006; Ji, 2008; Ji et al., 2009) or discrete element (Cook et al., 2004; Gil, 2005; Gil and Roegiers, 2006) approaches.

Most current hydraulic fracture models, particularly those that are based on the discrete fracture approach, assume a two-wing planar fracture that is believed to occur in competent rocks. Laboratory tests indicate that weakly consolidated sand formations are prone to shear failure/fracturing around water injection wells (Bohloli and de Pater, 2006), resulting in shear dilation; hence, higher permeability and higher compressive stresses around the wellbore. The shear failure process may lead to the formation of a fracture network instead of a planar tensile fracture commonly observed in hard rocks. The assumption of a two-wing tensile fracture with a well-defined fracture direction may not be an appropriate justification to simulate hydraulic fracturing in weakly consolidated sandstone formations. Therefore, new modeling approaches need to be developed.

Smear fracture modeling techniques are found to be more suitable than the discrete fracture modeling technique for hydraulic fracturing simulation in unconsolidated and weakly consolidated sandstones. However, there are limitations to some aspects of existing smeared fracturing models for hydraulic fracturing. They either do not distinguish between the flow conductivity of a shear failure/fracture and a tensile fracture (Xu, 2010) or they assign a constant permeability to the tensile fracture which is not a function of the fracture aperture (Zhai, 2006). However, the physics of fluid flow in tensile and shear fractures is different. In shear fracturing, the permeability of a rock matrix may increase due to the dilative rock deformation in the shearing process. A few permeability correlations have accounted for shear-enhanced permeability. Examples include Kozeny-Carman (Das, 2008) and the models presented by

Tortike and Ali (1993), Touhidi-Baghini (1998) and Wong (2003), which are presented in Table 1.

Table 1: Some Examples of Proposed Correlations for Shear Fracture Permeability Enhancement

Author	Correlation
Kozeny-Carman (mentioned in Das, 2008)	$\frac{k}{k_0} = \left(\frac{\phi}{\phi_0}\right)^3 \frac{(1 - \phi_0)^2}{(1 + \phi)}$
Tortike and Ali (1993)	$\frac{k}{k_0} = \frac{(1 + \varepsilon_v/\phi_0)^3}{(1 + \varepsilon_v)}$
Touhidi-Baghini (1998)	$\ln \frac{k}{k_0} = \frac{B}{\phi_0} \varepsilon_v$
Wong (2003)	$k_1 = k_1^0 + a(\varepsilon_1 + \varepsilon_3) + (b - a)\varepsilon_3$ $k_3 = k_3^0 + a(\varepsilon_1 + \varepsilon_3) + (b - a)\varepsilon_1$
Yuan and Harrison (2005)	$k = \frac{Vg}{48\mu} \varepsilon_v^2$

k_0 : initial permeability, k : enhanced permeability due to shearing, ϕ_0 : initial porosity, ϕ : enhanced porosity due to shearing, ε_v : volumetric strain, k_1^0 and k_3^0 initial principal permeabilities, ε_1 and ε_3 principal strains, a and b calibration parameters, V volume of degraded rock element, g gravitational acceleration, μ viscosity

Fluid flow in a tensile fracture can be considered as flow through an open space whereas flow in a shear fracture should be considered as flow through porous materials. For a tensile fracture, fluid flow can be modeled by using the parallel plate theory. In such cases, the fracture hydraulic conductivity is a function of the fracture's aperture. However, in a shear failure/fracture, the permeability of the sheared zone is a function of the fabric alteration and the dilative deformation of the shear fractures. In existing smeared fracture models, shear fractures are only simulated as diffused shear failure zones.

Assuming steady-state laminar flow of a Newtonian fluid between two parallel smooth plates (analogous to an ideal tensile fracture), the cubic law or parallel plate theory can be derived from the Navier-Stokes equations (Zimmerman and Bodvarsson, 1996; Waite et al., 1999; White, 2011). With the assumption of an incompressible fluid and no-slip boundary condition (meaning that the fluid velocity vector is equal to that of a solid at the solid-fluid boundary) (Zimmerman and Bodvarsson, 1996; Waite et al., 1999; White, 2011), the cubic law takes the form:

$$Q = C\bar{w}_f^3 \nabla h \quad (1)$$

where Q is the flow rate, C is a constant that represents the geometry of the flow, \bar{w}_f is the distance between the two plates (the fracture aperture), ∇ is the gradient operator and h is the hydraulic head.

Hydraulic conductivity of a fracture has been defined to be equivalent to the permeability parameter in Darcy's law for fluid flow in porous media (Zimmerman and Bodvarsson, 1996). From Eq. 1, the fracture conductivity, k_f can be related to the equivalent fracture permeability, as follows:

$$k_f = \frac{w^2}{12} \quad (2)$$

Sophisticated reservoir simulators should include not only the solution of fluid flow and stresses, but also the dependencies between the two. Such dependencies although ignored or approximated safely in elastic reservoirs, are pronounced in high-pressure injection operations like hydraulic fracturing and require the use of some sort of coupled geomechanics-fluid flow modeling. In petroleum-related operations, many of the processes and technical problems root in interactions between flow and stress-strain response of the formation. Injection of fluids and proppants into the hydrocarbon reservoirs during hydraulic fracture treatment induces significant variations in reservoir pressures which leads to the modification of the stress state in and around the reservoir. The reservoir properties like porosity and permeability could be altered by this change in the stresses which may, in turn, modify the fluid flow within the reservoir. This means that, in these situations, geomechanical effects (deformations and stresses) are strongly coupled to fluid flow. In numerical simulations, these interconnected effects should be captured and analyzed through the coupling of the geomechanics and reservoir fluid flow simulators.

There are many descriptions of such coupled simulators in the literature. As an example we can mention Settari and Mourits (1994) and Chin and Thomas (1999) in investigation of the effects of reservoir compaction, Chin et al. (1998) in the context of reservoir stress dependent permeability, Gutierrez and Makurat (1997) for studying fracture permeability variation of fractured reservoir, Behr et al. (2006) in the study of damage zone around a hydraulically fractured tight gas reservoir, and Miranda et al. (2010) in the study of hydraulic fracturing. Previous works have proved that coupling of the reservoir simulation and geomechanics modeling is essential in better understanding of the hydraulic fracturing treatment. The coupling

of fracture propagation with reservoir fluid flow and heat transfer were mathematically established first in 1980s (Hagoort et al, 1980; Settari, 1980; Nghiem, 1984), and more recently in Faisal et al. (2004) or Longuemare (2001). In the early works, essentially two independent grid systems were used for the numerical solution of the continuity equation in the fracture and the partial differential equations for the reservoir multi-phase flow. The coupling was improved later on by using only one set of common gridblocks for both fracture and reservoir flow and considering a high permeability for the fracture (Settari et al, 1990; Weill and Latil, 1992). Further improvement was achieved by using pressure/stress dependent permeability in the coupled simulations (Garon and Dunayevsky, 1988; Settari and Mourits, 1994, 1998; Ji et al., 2004, 2006). Lebel (2002) used a type of upstream weighting in evaluating the effective permeability between fractured gridblocks. Hustedt et al. (2005) used a two-way explicit coupling approach between a reservoir simulator and a fracture simulator which was proposed by Hoek et al., earlier in 1996 but was using a pseudo 3-D fracture model. Ehrl (2000) optimized future field development by integrating a 3-D geologic model and a field-scale reservoir simulation model in which local grid refinements were used around the wells to remove numerical stability problems. However, the most flexible approach was suggested by the use of partially de-coupled approach (Settari et al, 1990; Weill and Latil, 1992).

Although most of the field evidence are related to the importance of coupling in unconsolidated or soft formations, where the reservoir undergoes large rock deformation, Heffer et al. (1994) showed that coupling effects can also be significant in fractured reservoirs.

Historically, numerical modeling of such coupled processes were performed in a fully decoupled manner and based on the primary purpose of the computation, were categorized into geomechanical modelling, reservoir simulation and fracture mechanics with the primary goal of computation as stress-strain behavior, flow in porous media and fracture propagation, respectively. Simplifying assumptions were inevitable about part of the problem that was not of primary interest. It is obvious that such an approach proves to be inadequate in situations where strong coupling between these processes exists. As an example, porosity and permeability of the formation may change in any type of reservoir modelling of fluid injection into the wellbore, due to the stress changes and failure of the underground formation.

Generally, the linkage between the simulators falls within three main categories. It can be either a fully decoupled type linkage, a fully coupled type or partially decoupled. In the first two

types of linkage, an explicit fracture is simulated in the model, but in the third approach, some sort of “effect” of the fracture is included. Here we don’t discuss fully coupled models since we are using a multi-module simulator and different modules are linked together through partially coupled principals. This approach seems to be effective when we consider proliferation of the available geomechanics codes outside the petroleum engineering. Our in-house developed fluid flow simulator, which is coded in MATLAB, is the host and is linked to the commercial stress simulator FLAC to develop our numerical hydraulic fracture simulator.

Partially decoupled approach, which was utilized in this study, falls in between the other two approaches in which the fracture propagation and reservoir fluid flow are solved independently. However, the results from each module is transferred to the other simulator to improve the outcome. In this approach, the new fracture grids can be easily generated and, in principal, it can be conveniently attached to any type of reservoir or fracture simulator. This greatly increases the flexibility and range of application of the method. Settari (1988) was the first researcher who proposed this modular coupling. In modular coupling information is passed between different modules and iterations are used to converge the solution. Such an approach can even use highly advanced commercial reservoir and geomechanics simulators.

Models can be built based on solving the fluid flow and stress equations in different modules. Our model consists of three separate simulators: fluid flow, geomechanics and proppant. In modular simulators, different strategies are applied to link the modules namely, “one way coupling”, “loose (explicit or sequential) coupling” and “iterative coupling” (Settari and Walters, 2001).

2. Model Formulation

Our hydraulic fracture numerical simulator consists of two modules: fluid flow and geomechanics. From now on, when we use the term “hydraulic fracture module”, we refer to the coupled fluid flow and geomechanics modules.

Fluid flow simulator is the host or master module in the iteratively coupled model, which means it is run in the beginning of each time step and it triggers (calls) the geomechanics module to calculate stresses and displacements. In practice, the iterative modular coupling has a great range of flexibility since each of the modules can be any commercial software.

It is well known that the orientation of the hydraulic fracture is determined by the in-situ stress field: the hydraulic fracture will propagate perpendicular to the minimum principal in-situ stress. In all of our simulations, we assumed the minimum principal stress is horizontal; therefore, the fracture plane is a vertical plane, normal to the direction of minimum stress.

For simplifying the illustrations, we assume that the minimum in-situ stress is along y direction and compressive stresses are negative.

2.1 Fracture Detection and Dimensions

There are many different fracture initiation and propagation criteria in the literature. In this work, we utilized the geomechanical results for this purpose and assumed that fracture initiation and propagation are determined by the effective stresses. The fracture initiation and propagation in this work are assumed to occur when the tensile stress exceeds the tensile strength of the rock:

$$\sigma_3 + p \geq \sigma_T \quad (3)$$

where σ_3 is the minimum principal stress, p is the pore pressure and σ_T is tensile strength of the rock.

Due to the fluid injection and poro-elastic/plastic effects, the stress at the fracture tip is changing with time. This change varies along the model and is generally complex. Hence, we reformulate the initiation and propagation criterion as:

$$\sigma_{tip} + p \geq \sigma_T \quad (4)$$

where σ_{tip} is the minimum principal stress at the tip of the fracture. This equation means that fracture will propagate through a gridblock if the least principal effective stress at that gridblock exceeds the tensile strength of the rock. This criterion is checked in every time step in the geomechanical module to give the dimensions of the fracture.

The total length of the fracture is determined by the sum of the length of all the gridblocks that satisfy Eq. 4 criterion. The height of the fracture is assumed to be equal to the pay thickness.

The width on the other hand can be calculated from geomechanics. If the initiation criterion is met in any gridblock, then the width of the fracture at the corresponding location is determined from nodal displacement of that gridblock in the direction normal to the minimum principal stress, as:

$$w(x, y) = 2u_y(x, y) \quad (5)$$

where w is fracture width and u_y is displacement perpendicular to the minimum principal stress.

2.2 Material Constitutive Model

A bilinear Mohr-Coulomb shear model with strain hardening/softening was employed in the model to describe the material constitutive behavior. The yield surfaces can be expressed in the following form (Nouri et al., 2009; Jafarpour et al., 2012):

$$F = T - (q + P)\mu = 0 \quad (6)$$

where P is the mean effective stress, and T is the square root of the second invariant of the deviatoric stress tensor in an axisymmetric state of stress (as in a triaxial compression experiment). P and T are defined as:

$$P = \frac{(\sigma'_z + 2\sigma'_r)}{3} \quad (7)$$

$$T = \frac{|\sigma'_z - \sigma'_r|}{\sqrt{3}} \quad (8)$$

and μ is the friction coefficient which is equal to $\tan(\phi_\sigma)$. This parameter is related to the friction angle (ϕ_σ) in the following form:

$$\tan \phi_\sigma = \frac{2\sqrt{3} \sin \phi_a}{3 - \sin \phi_\sigma} \quad (9)$$

The rock is assumed to undergo linear softening under tension before fracturing (Fig. 1). The tensile fracturing criterion is consistent with the model that Papanastasiou (1997b) and Papanastasiou (1999) used for the interface elements lying in the crack-growth direction (Fig. 1). In this model, the energy release rate (G_{IC}), is equal to the area under the stress-displacement curve. In Fig. 1, σ_T is the uniaxial tensile strength, δ_C is the critical opening displacement at which effective stress falls off to zero and G_{IC} is Mode I critical energy release rate. The values of G_{IC} and σ_T will be given as input to the model so that stress-displacement curve can be determined.

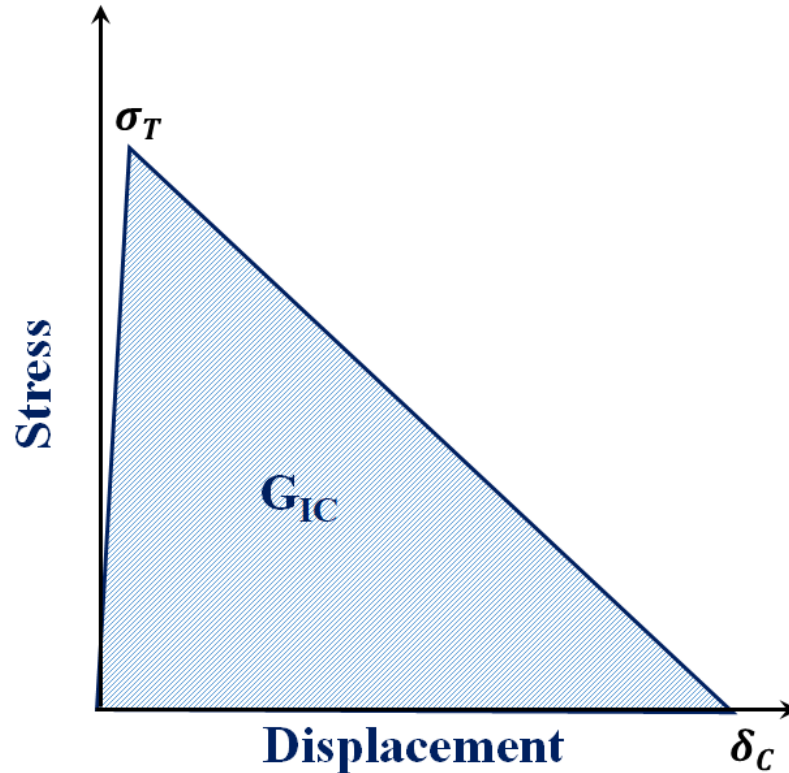


Figure 1: Cohesive Behavior of Fracture

2.3 Calculation of the Average Permeability in Fractured Gridblocks

In our hydraulic fracture simulator, only one common grid system is considered for both the reservoir and the fracture. If the fracture is modeled with its actual dimensions, a severe time step limitation arises in the simulation. Correspondingly, the permeability and porosity of the fracture is smeared in the encompassing gridblock. Based on the fluid flow cubic law, the permeability of the fracture depends on the fracture aperture or width according to Eq. 2.

This equation gives a large value for the permeability and, therefore, the fracture is the highly permeable part of the encompassing gridblock. For this reason, the permeability of the fractured gridblocks should be enhanced to include the effect of fracture on fluid flow.

2.4 Permeability Enhancement for Grids Completely Penetrated by Fracture

All the gridblocks in the reservoir simulator that contain the fracture will be completely penetrated by the fracture, except for one gridblock that contains the fracture tip. Obviously, the presence of fracture results a significant permeability enhancement. However, in smeared fracture approach, this enhancement should be averaged within the whole gridblock.

There are two flow paths between adjacent blocks, namely through the fracture and through the matrix. Therefore, the total flow from grid i to $i+1$ will be the sum of the flow through matrix and fracture:

$$q_t = q_m + q_f \quad (10)$$

where q_m is the matrix flow rate and q_f is the fracture flow rate. According to Darcy's law, each of these flow rates can be stated as:

$$q_t = \frac{k_{avg}\Delta y\Delta z}{\mu B\Delta x} (p_{i+1} - p_i) \quad (11)$$

$$q_m = \frac{k_m(\Delta y - w)\Delta z}{\mu B\Delta x} (p_{i+1} - p_i) \quad (12)$$

$$q_f = \frac{k_f w\Delta z}{\mu B\Delta x} (p_{i+1} - p_i) \quad (13)$$

Substituting Eq. 11 to 13 into Eq. 10 gives the average permeability of the fractured block as:

$$k_{avg} = \frac{k_m(\Delta y - w) + k_f w}{\Delta y} \quad (14)$$

k_{avg} is the permeability of the gridblock that contains the fracture. The fracture width is usually ignored in the matrix flow rate calculation since it is generally much smaller than Δy of element. However, we keep this term in all the formulations.

Fracture permeability is a function of aperture and aperture is a function of net pressure inside the fracture (or effective stress). Therefore, it can be concluded that above treatment makes the permeability pressure-dependent or effective stress-dependent. In addition, in our numerical simulations, such a dynamic calculation of permeability through time can be used to capture the change of matrix permeability due to pore pressure changes during injection (or production) in stress sensitive formations or change in fracture mobility due to proppant injection.

The permeability enhancement can be applied in explicit or implicit ways. Explicit treatment of permeability enhancement means evaluating average permeabilities based on fracture dimensions at previous time step. The amount of permeability enhancement is calculated only once at the beginning of each time step and it will not change during iterations:

$$k_{avg}^{n+1} = \frac{k_m(\Delta y - w^n) + k_f^n w^n}{\Delta y} \quad (15)$$

Implicit treatment, however, means that the average permeability is calculated from latest iteration level of the fracture dimensions:

$$k_{avg}^{n+1} = \frac{k_m(\Delta y - w^{n+1}) + k_f^{n+1} w^{n+1}}{\Delta y} \quad (16)$$

where v denotes iteration level and n shows step time level.

Ji (2008) reported that explicit treatment of permeabilities causes oscillations while the implicit treatment generates smoother results in length and in pressures. Therefore, for all HF simulations in this research, an implicit treatment of permeabilities (Eqs. 25) was adopted.

2.5 Smeared Shear Failure Flow Model

Once a tensile fracture is detected in an element in any time step in the model, the permeability of that element is modified using the cubic law for the smeared fracture (Eq. 14). This multiplier is applied to the permeability in the fracture direction, while the permeability in the direction normal to the fracture remains unchanged or follows the shear permeability criteria if shear failure is detected. This orthotropic permeability tensor is then rotated back to the global coordinate system, resulting in the anisotropic permeability tensor for the fractured element.

Touhidi-Baghini's model (1998) in the form of Eq. 17 with different B values in horizontal and vertical directions was used to describe the shear permeability enhancement in the developed hydraulic fracture model.

$$\ln \frac{k_{ij}}{k_{0ij}} = \frac{B}{\phi_0} \varepsilon_v \quad (17)$$

where k_{ij} and k_{0ij} are the evolved and initial permeability of the element, respectively, ε_v is volumetric strain and B is the rate at which permeability evolves as a function of volumetric strain variance.

2.6 Porosity Change

During fluid injection into the formation, porosity of the formation rock changes. It is desirable to state this change of porosity in terms of volumetric strains, so that the direct outputs of geomechanics module can be used to obtain the new porosity value in each time step. Assuming the original porosity of the formation is:

$$\phi_0 = \frac{V_t - V_g}{V_t} \quad (18)$$

where V_t is the total volume and V_g is grain volume, if any volume change, ΔV , occurs, the new porosity will be:

$$\phi_{new} = \frac{(V_t + \Delta V) - V_g}{(V_t + \Delta V)} \quad (19)$$

The volumetric strain, ε_v , on the other hand is:

$$\varepsilon_v = \frac{\Delta V}{V_t} \quad (20)$$

Therefore:

$$\phi_{new} = \frac{(V_t + \varepsilon_v V_t) - V_g}{(V_t + \varepsilon_v V_t)} \quad (21)$$

or:

$$\phi_{new} = \frac{\varepsilon_v + \phi_0}{1 + \varepsilon_v} \quad (22)$$

This change in porosity is due to the deformation of the rock. On the other hand, fracture porosity also needs to be included in the porosity calculation of the fracture gridblocks. Fracture volume in a given gridblock can be calculated as:

$$V_f = L_{f_i} \Delta z w \quad (23)$$

where L_{f_i} is the fracture length in the gridblock. Therefore, the fracture porosity is:

$$\phi_f = \frac{V_f}{V_b} = \frac{L_{f_i} \Delta z w}{\Delta x \Delta z \Delta y} = \frac{L_{f_i} w}{\Delta x \Delta y} \quad (24)$$

where V_b is the bulk volume of the gridblock. The total porosity of a fractured gridblock will be:

$$\phi = \frac{\varepsilon_v + \phi_0}{1 + \varepsilon_v} + \frac{L_{f_i} w}{\Delta x \Delta y} \quad (25)$$

By treating porosity in this way, any closing or opening of the fracture which in turn results in fracture volume change, can be captured as a change of fracture porosity.

2.7 Fluid Flow Model

As it was mentioned in Section 2.6, the full permeability tensor is generated during tensile and shear failure of material in the model. Darcy's law for fluid flow in porous media is used to solve the flow in the intact matrix, tensile fractures and shear failure:

$$q_i = - \frac{k_{ij} \partial p}{\mu_f \partial x_j} \quad (26)$$

where q_i is the specific discharge vector, k_{ij} is the full tensor permeability, μ_f is the fluid viscosity, p is the fluid pressure and $i, j = 1, 2$ are indexes for two-dimensional analysis.

3 Iterative Coupling between Fluid Flow and Geomechanics Modules

This section presents our numerical technique in developing a hydraulic fracture simulator through iterative coupling of a reservoir simulator and an advanced commercial geomechanics software, FLAC 2D, with considering plasticity effects.

The type of coupling that we used is “iterative coupling” in which iteration is carried out, in each time step, between the fluid flow and geomechanics modules until certain convergence criteria are met. In each iteration, the previous guess of the permeability and porosity is used to solve the flow equation and the corresponding change of pore pressure is used to calculate new deformations and stresses, which in turn provide new update of permeability. Iterative coupling, when converged, gives equivalent solution to a fully coupled model, while it is much more flexible and less computational demanding (Settari and Mourits, 1998).

Each of the abovementioned strategies of partially coupled models can be performed in two ways: “Pore Volume Coupling” and “Flow Properties Coupling” (Settari and Mourits, 1998). The information that is updated and transferred to the other module is different in these two methods. Flow properties coupling was implemented in our linkage algorithm and therefore will be described in detail in this section.

In flow properties coupling, permeability is modified as a function of effective stresses. Such a relationship has been investigated for many types of formation rocks and is stronger in low permeability materials. In the traditional approach of flow dependent coupling, tables of primary flow property, which is permeability, versus pressure is used in an uncoupled model. In those approaches, different assumptions are made about stress change during time. However, in the modern attempts of this type of coupling, stresses are obtained by including geomechanics equations. The main advantage of such coupling is its capability in predicting permeability changes from the geomechanics of opening fractures or failure (dilation) of joints. The orientation of fractures or joint requires full tensor permeability in the flow model. Consequently, flow properties coupling, can capture the change in reservoir description through time because of geomechanics. In hydraulic fracturing simulation, the transmissibility multiplier in the potential fracture plane is dynamically changed and the changes in fracture propagation pressure with time, which may be large, can be captured.

Only one grid system is used for reservoir simulation and geomechanics modeling to better evaluate the mutual influence between dynamic fracture propagation and fluid flow. Although, in theory, the stress model can have an independent mesh from the reservoir simulator mesh, it is advantageous and simpler to use the same mesh for the two modules. In this case, since the location of the nodes are the same in the two gridding systems, there is no need to map the

results from one grid system to another. The zero-displacement boundaries of the model are placed far enough from the well such that they do not influence the solution.

The communication between the simulators takes place through an interface code developed in MATLAB. The pressure changes occurring in the reservoir simulator are passed to the geomechanical simulator by the interface code and the updated stresses and displacements are passed back to the reservoir simulator and are used to evaluate coupled parameters in the reservoir formulation. Iterations are needed to ensure convergence. The interface code has enough flexibility to allow different degrees of coupling depending on the accuracy needed.

As it can be concluded from presented formulation of permeability and porosity, a strong dependency exists between fluid flow and geomechanics outputs; therefore, the linkage between the modules is essential. In our coupling scheme, porosity and permeability are used as the coupling parameters between the modules.

After creating model geometry and the mesh, fluid flow simulator starts the simulation to give pore pressures of the gridblocks. These pressures are transferred to the geomechanics module in which stresses and strains are calculated. The pore pressures are used to calculate effective stresses and check the fracture initiation and propagation criteria (Eq. 4). If the criteria are met in any gridblock, it is marked as fractured. Next, Eq. 5 is used to obtain fracture geometry. This geometry is used to update the permeability of the gridblocks that contain the fracture, according to permeability sensitive laws described in Eq. 14. Also, porosity of the gridblocks is modified according to Eq. 25. Using the updated permeability and porosity, the reservoir simulator is run again, for the same time step, but next iteration to improve pore pressure results. This process is repeated until the maximum change in pore pressure, porosity, permeability and width falls below a certain level.

4. Verification of the Hydraulic Fracture Model

The above formulation of permeability enhancement in fractured gridblocks was tested in a simulation of an isothermal reservoir with single-phase, slightly compressible fluid flow. A static fracture was represented in the model by assigning higher values of permeability to the gridblocks containing the fracture. Analytical solution of such a problem exists in the literature and it is used as a validation to the permeability modification of our numerical tool. The problem description is as follows:

Figure 2a shows a schematic view of the reservoir simulation problem that was used for our validation purposes. A horizontal, homogeneous, isotropic reservoir saturated with slightly compressible fluid is considered. Gravity effects are neglected, and the reservoir is at an initial pressure of p_i . The well is assumed to be in a rectangular drainage area. A vertical fracture is assumed extending over the entire height of the formation, which is parallel to the drainage boundary and is located symmetrically within the square drainage area. In the numerical model, a homogeneous, isotropic, square drainage model filled with slightly compressible fluid of constant viscosity was created. The fracture was assumed to be in the center of the model, as shown in the Fig. 2a. Table 2 shows the input data used in the model.

Table 2: Input Parameters for Infinite Conductivity Fracture Simulation

Parameter	Value
Porosity	0.25
Permeability	$0.9869 \times 10^{-13} \text{ m}^2$ (0.1 Da)
Viscosity	1 cp (0.001 Pa.Sec)
Fluid Compressibility	$1 \times 10^{-10} \text{ Pa}^{-1}$
Injection Flow Rate	$8 \times 10^{-5} \text{ m}^3/\text{Sec}$
Reservoir Dimensions (Drainage Area)	300 m by 300 m (90000 m^2)
Reservoir Height	1 m
Initial Reservoir Pore Pressure	5 MPa
Grid Size	2.9412 m \times 5.8824 m
Grid Number	51 by 51
Fracture Width	0.001 m
Fracture Half Length	Variable

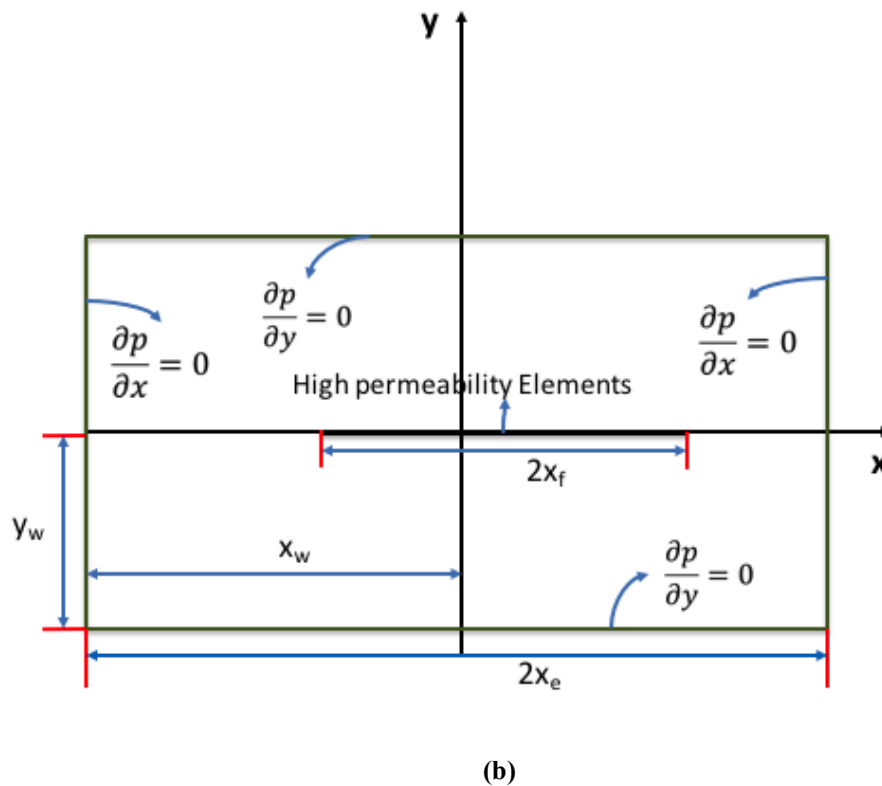
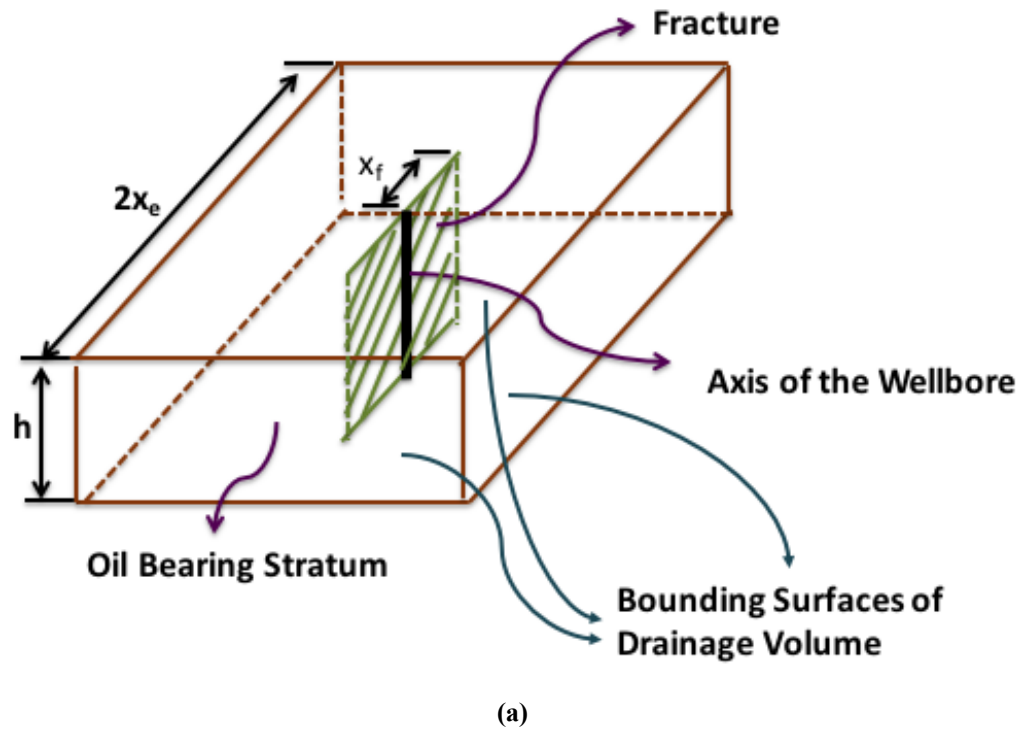


Figure 2: (a) Schematic View of Fractured Well and Reservoir Drainage Volume; (b) Plan View of the Fractured Reservoir

The boundary conditions that complete our problem are no flow boundary around the model.

Gringarten (1974) by using Green's function and product solution method obtained the analytical solution to pressure distribution in the abovementioned problem as:

$$\begin{aligned}
p_D\left(\frac{x}{x_e}, \frac{y}{y_e}, t_{DA}\right) & \quad (27) \\
= 2\pi \int_0^{t_{DA}} & \left[1 + 2 \sum_{n=1}^{\infty} e^{-n^2\pi^2\frac{x_e t'_{DA}}{y_e}} \cos\left(n\pi \frac{y_w}{2y_e}\right) \cdot \cos\left(n\pi \frac{y_w + y}{2y_e}\right) \right] \left[1 \right. \\
+ 2 \sum_{n=1}^{\infty} & e^{-n^2\pi^2\frac{y_e t'_{DA}}{x_e}} \frac{\sin\left(n\pi \frac{x_f}{2x_e}\right)}{n\pi \frac{x_f}{2x_e}} \cdot \cos\left(n\pi \frac{x_w}{2x_e}\right) \cdot \cos\left(n\pi \frac{x_w + x}{2x_e}\right) \left. \right] dt'_{DA}
\end{aligned}$$

where:

$$t_{DA} = \frac{kt}{4\mu c\phi(x_e y_e)^2} \quad (28)$$

and

$$p_D(x_D, y_D, t_D) = \frac{2\pi kh}{q\mu} (p - p_i) \quad (29)$$

x_e and y_e are half length of reservoir drainage area and x_w and y_w show fracture axis coordinates (see Fig. 2b), and p_i is the initial reservoir pressure. Therefore, the pressure drop at the center of a square drainage area ($x_e = y_e, x_w = y_w$) is:

$$\begin{aligned}
p_{wD}(t_{DA}) & = 2\pi \int_0^{t_{DA}} \left[1 + 2 \sum_{n=1}^{\infty} e^{-4n^2\pi^2 t'_{DA}} \right] \left[1 \right. \\
& \quad \left. + 2 \sum_{n=1}^{\infty} e^{-4n^2\pi^2\frac{y_e t'_{DA}}{x_e}} \frac{\sin\left(n\pi \frac{x_f}{x_e}\right)}{n\pi \frac{x_f}{x_e}} \cdot \cos\left(n\pi x_D \frac{x_f}{x_e}\right) \right] dt'_{DA} \quad (30)
\end{aligned}$$

The pressure drop on the fracture can be obtained by setting $x_D = 0$ in Eq. 30. Gringarten also presented numerical results of above function which we have used for validation. Figure 3a is a graphical representation of the analytical solution of Gringarten.

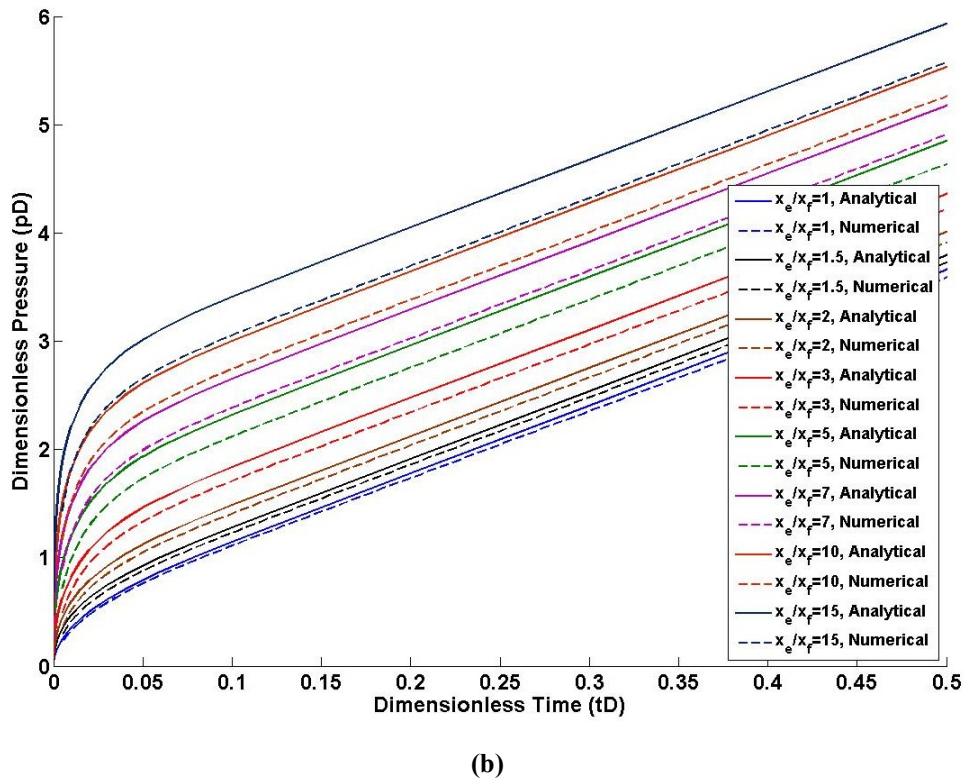
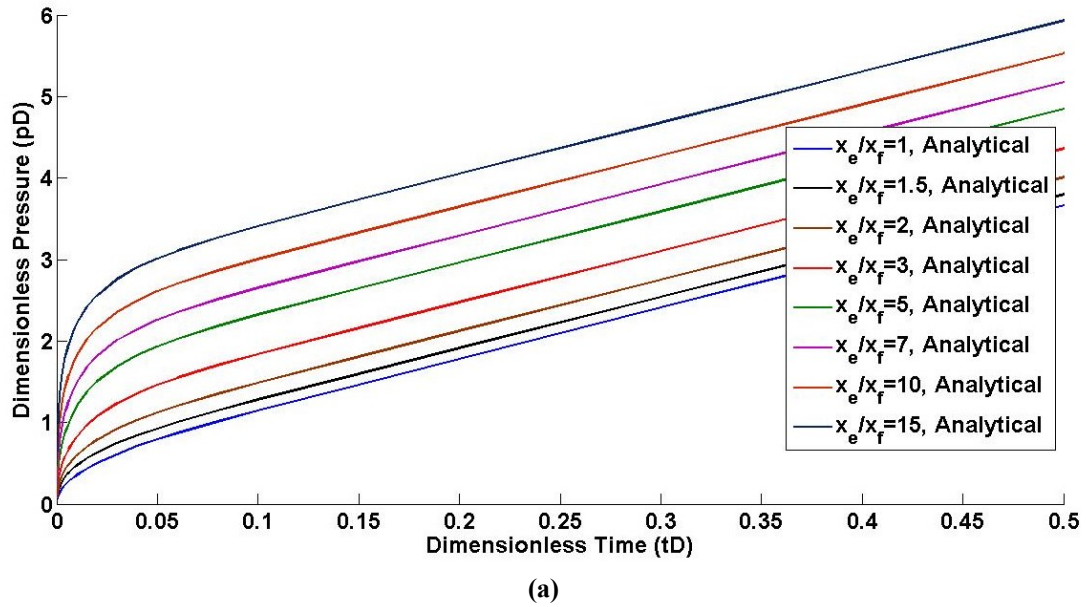


Figure 3a: Graphical Representation of Gringarten Solution; (b) Comparison of Gringarten Analytical Solution with Numerical Simulation

Figure 3b presents a comparison between the dimensionless pressure drops from the numerical model and the analytical solution of Gringarten (1974). The results indicate that permeability enhancement method gives accurate results which match reasonably well and within 5% difference with the analytical solutions.

4.1 Effect of Local Grid Refinement

A mesh sensitivity analysis is performed in this section to investigate the effect of different meshing strategies on the pressure response. The model input parameters are the same as in Table 2 and it is assumed that the ratio of reservoir drainage length to fracture length is 5 ($x_e/x_f=5$). In some of the simulations of this part, uniform grids are used, but the size of the grid is changing in each case. In the non-uniform case mesh (71 by 71), a locally refined mesh is designed in which the size of the mesh in an 11-meter band around the injection point is about 1 m by 1 m and then increases to 5 m by 5.5 m around the refined band, as shown in Fig 4.

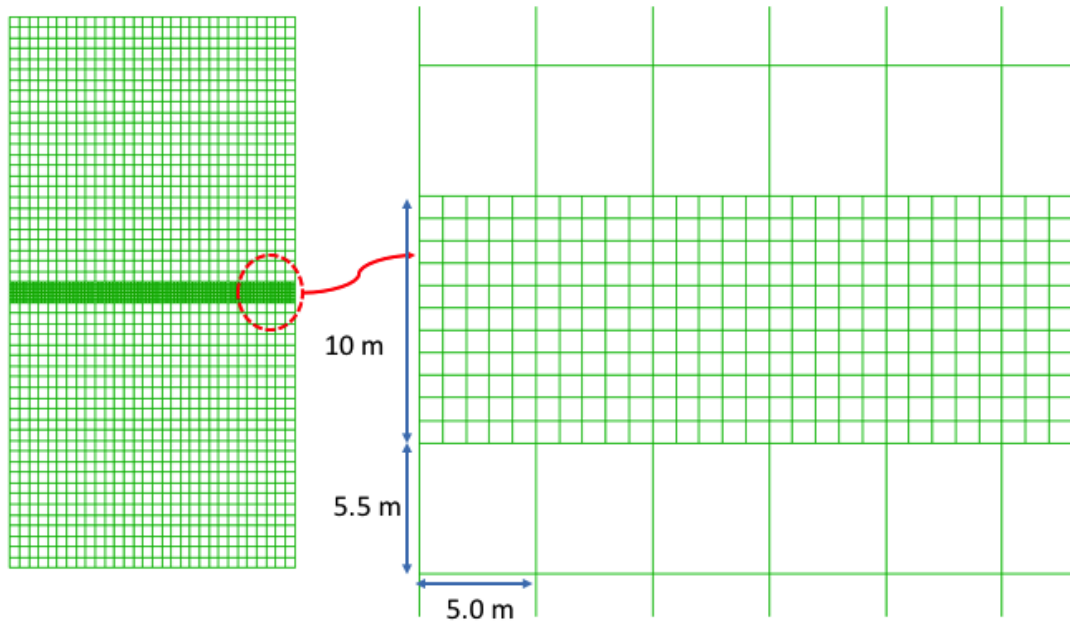
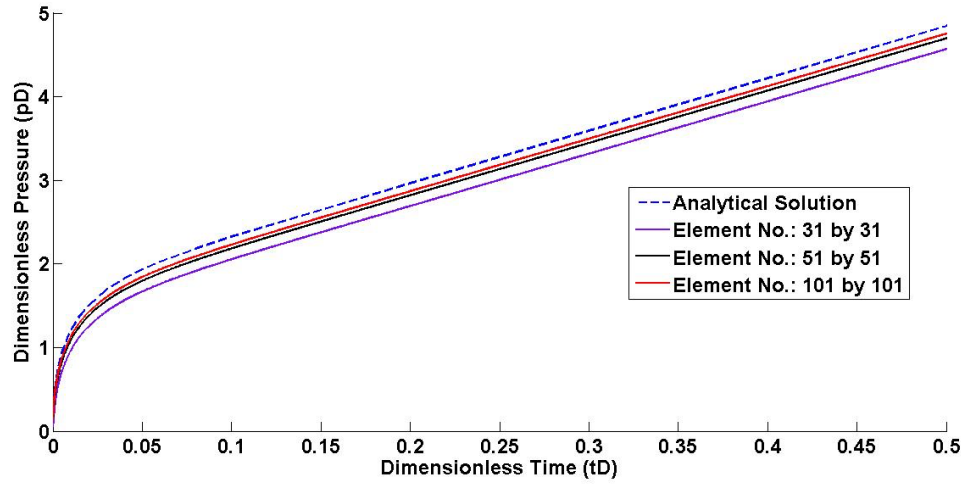
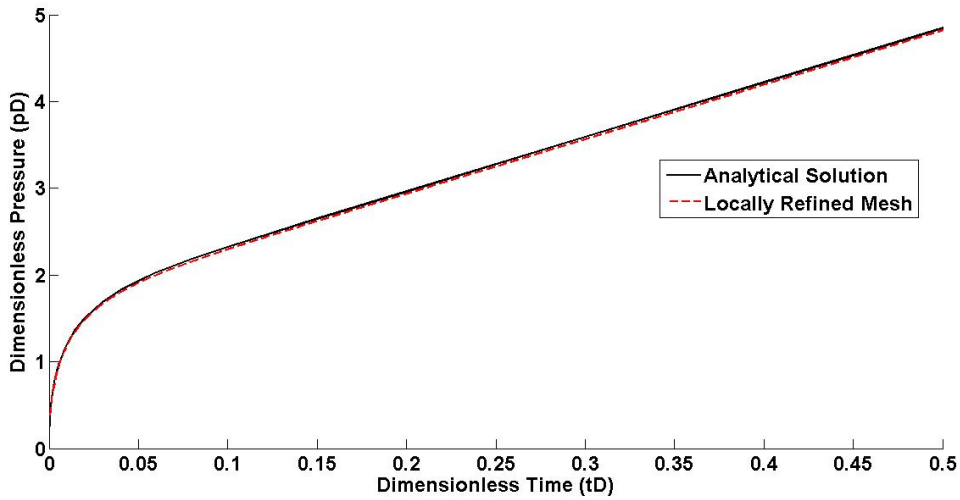


Figure 4: Locally Refined Mesh

As seen from Fig. 5a, as the size of the gridblock becomes smaller, the pressure response becomes closer to the analytical solution. However, when uniform grids are used, running time of the simulation becomes too expensive and still the accuracy is not desirable. On the other hand, locally refined mesh gives a high accuracy with manageable running time, as shown in Fig. 5b.



(a)



(b)

Figure 5: (a) Effect of Uniform Size Mesh Refinement; (b): Effect of Locally Refined Mesh

4.2 Effect of Maximum Limit of Permeability

The higher the permeability of the fracture, the less the friction loss inside the fracture will be. However, it is recognized that after a certain value of permeability, increasing this parameter does not change the fracture behavior. It is because when permeability of the fracture is much higher than the matrix permeability, the majority of fluid passes through the fracture. It is well known that the permeability of the fractured elements should be gradually increased in each iteration or otherwise severe oscillations will arise (Ji, 2008). Obviously, higher value of permeability of the fracture requires higher number of iterations to bring matrix permeability to fracture permeability. Setting a maximum limit for permeability in our numerical work reduces the number of iterations and consequently running time. Therefore, it is worth to investigate the

fracture permeability that leads to solutions that match reasonably well with those obtained from a model with “infinite conductivity” fracture. We investigated the effect of setting a maximum limit of permeability, both for static and dynamic fractures.

The static fracture model is the same as the model explained in Section 5. Figure 6 shows how the change of maximum permeability of the fracture changes the injection pressure. As the maximum limit of permeability is increasing, the pressure at the wellbore decreases and gets closer to the analytical solution. However, since we are using smeared approach in simulating the fracture, the numerical results and analytical solutions will never match unless a very fine grid is used.

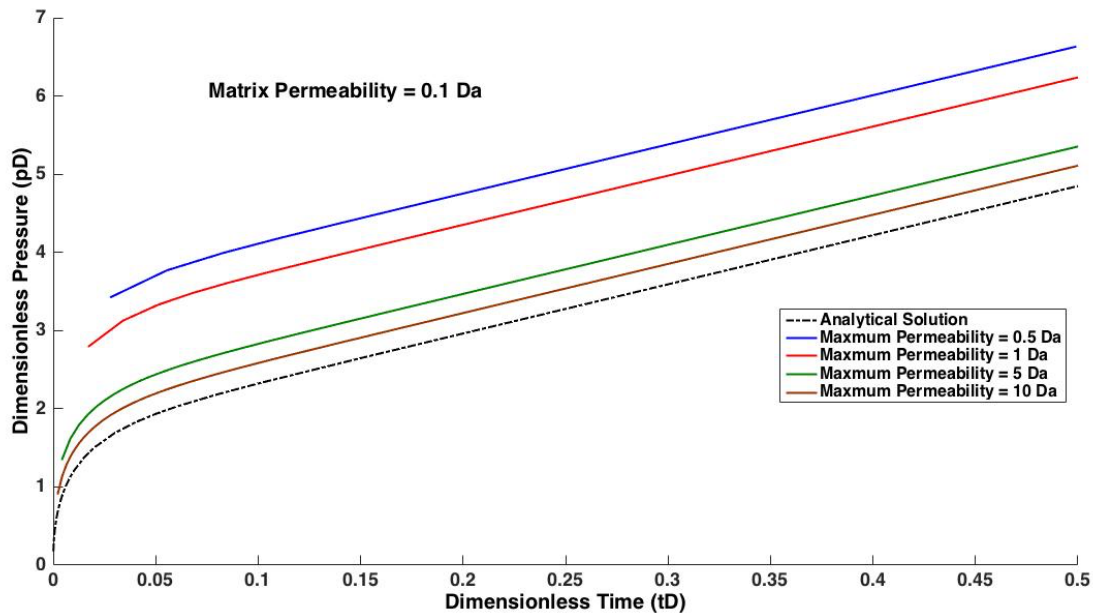


Figure 6: Effect of Maximum Permeability Limit on Static Fracture

For the case of dynamic fracture propagation, a 50 m by 50 m model was built and geomechanics and fluid flow modules were linked as explained in Section 3. Table 3 presents the input parameters of the model. It is assumed that formation rock follows Mohr-Coulomb plasticity model and water is used as injection fluid.

Table 3: Input Parameters for Dynamic Fracture Model

Parameter	Value
Model Dimensions	100 m by 50 m
Injecting Fluid Viscosity	0.001 Pa.Sec.
Formation Initial Porosity	0.2

Formation Initial Horizontal Permeability	0.1 Da
Formation Initial Vertical Permeability	0.1 Da
Initial Reservoir Pressure	1.6 MPa
Young's Modulus	1.785 GPa
Poisson's Ratio	0.3
Vertical Principal Stress	4 MPa
Maximum Horizontal Principal Stress	6.7 MPa
Minimum Horizontal Principal Stress	3 MPa
Cohesion	1.185 MPa
Friction Angle	20
Dilation Angle	22
Fracture Toughness	1 MPa. \sqrt{m}
Injection Time	2000 Seconds

Figure 7 displays the boundary conditions of the geomechanics and fluid flow simulators.

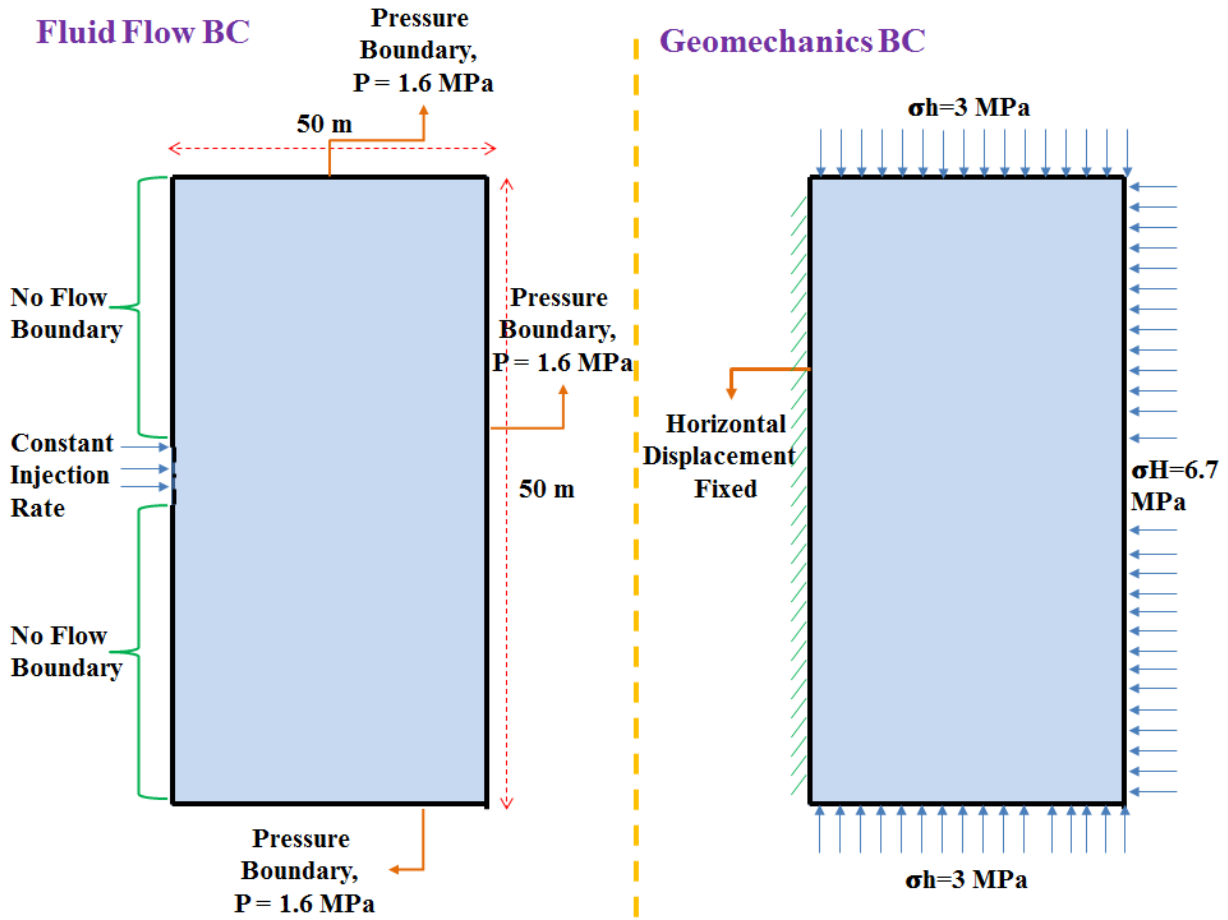
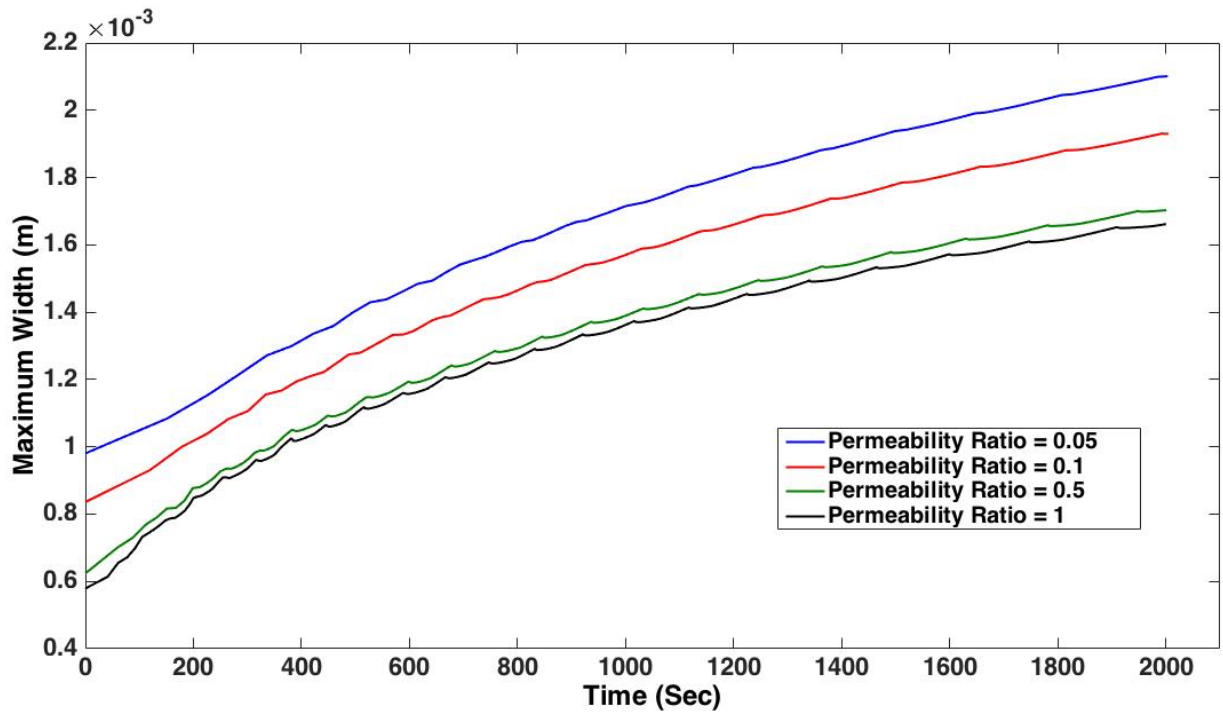


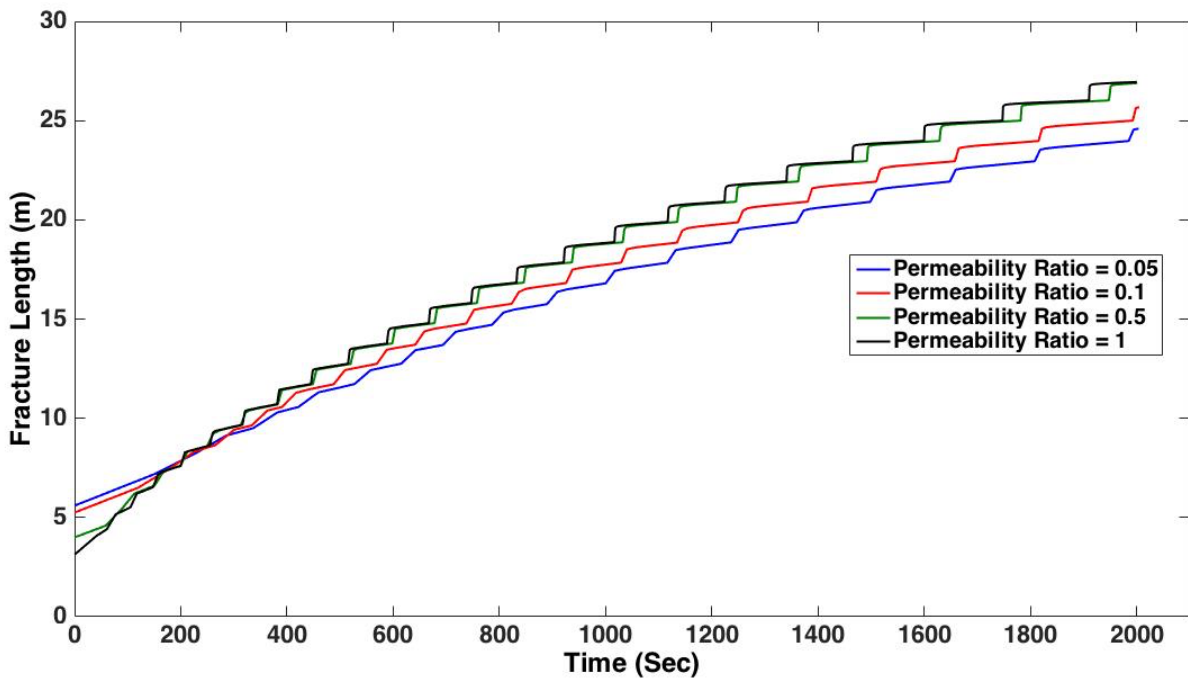
Figure 7: Fluid Flow and Geomechanics Boundary Conditions

In dynamic fracture case, the width changes along the fracture length and, therefore, a variable permeability limit should be assigned to fractured elements. In Figs. 8a and 8b, permeability ratio means the ratio of the assigned permeability in the numerical code to the actual smeared permeability coming from Eq. 14.

Figure 8a compares the maximum width of the fracture while Fig. 8b shows fracture length for different maximum limits of permeability. Again, negligible differences are obtained between the results even when a limit is assigned to the maximum permeability. However, in the dynamic fracture model, assigning a value of 0.05 to permeability ratio, lead to completely different results. Therefore, whenever fracture propagation is occurring inside the model, the maximum limit for permeability should be applied with some care.



(a)



(b)

Figure 8: (a) Effect of Maximum Permeability Limit on Fracture Width; (b) Effect of Maximum Permeability Limit on Fracture Length

5. Field Application

This section presents the numerical model design and input data for a series of well tests conducted at the Burnt Lake project (Xu, 2010). The project is located about 300 km northeast of Edmonton (Yeung and Adamson, 1991; Yeung, 1995). Cyclic steam stimulation was first proposed as the oil recovery scheme for this project to produce crude bitumen from the Clearwater formation in the Cold Lake oil sands deposit. Due to low heavy oil prices in the late 1980s, the project was suspended in 1989 and alternative lower-cost recovery methods were studied (Yeung and Adamson, 1991; Yeung, 1995).

Yeung (1995) and Xu (2010) provided some information on the geology of the project site, which is summarized here. The target zone of this project was in Clearwater B sand with a thickness of 20 to 30 meters. No gas cap was detected in the logs. In addition, no bottom water was detected except at the extreme northeast corner of the lease property. Clearwater B sand is fine-grained and unconsolidated sand consisting of 20% quartz, 20% feldspar and 60% rock fragments. Smectite, Illite, Chlorite and Kaolinite comprise about 10 to 20 % of the bulk volume.

The overlying layer is water-bearing Clearwater A sand, which is separated from Clearwater B by 4 to 5 meters of shale. Underlying the reservoir is shaly Clearwater C, which is very fine sand with interlayers of silt. Clearwater B and C are separated with a three-meter shale layer (Yeung, 1995).

Three well tests were performed in a cased well in the Burnt Lake project (well 01-14-67-03W4, Xu, 2010). The well tests were performed in a 178- millimeters diameter wellbore which was perforated in a five-meter interval in the middle of the pay zone (Clearwater B). The tests were conducted at different injection rates. The highest pressure was exercised in Test 3 and the lowest in Test 1. For each test, water was injected into the oil sand formation for a specific period, and the well was then shut in until the bottomhole pressure returned to the static level. The bottomhole pressure was recorded during the test (Xu, 2010). The bottomhole pressures and flow rates for all three well tests are shown in Fig. 9.

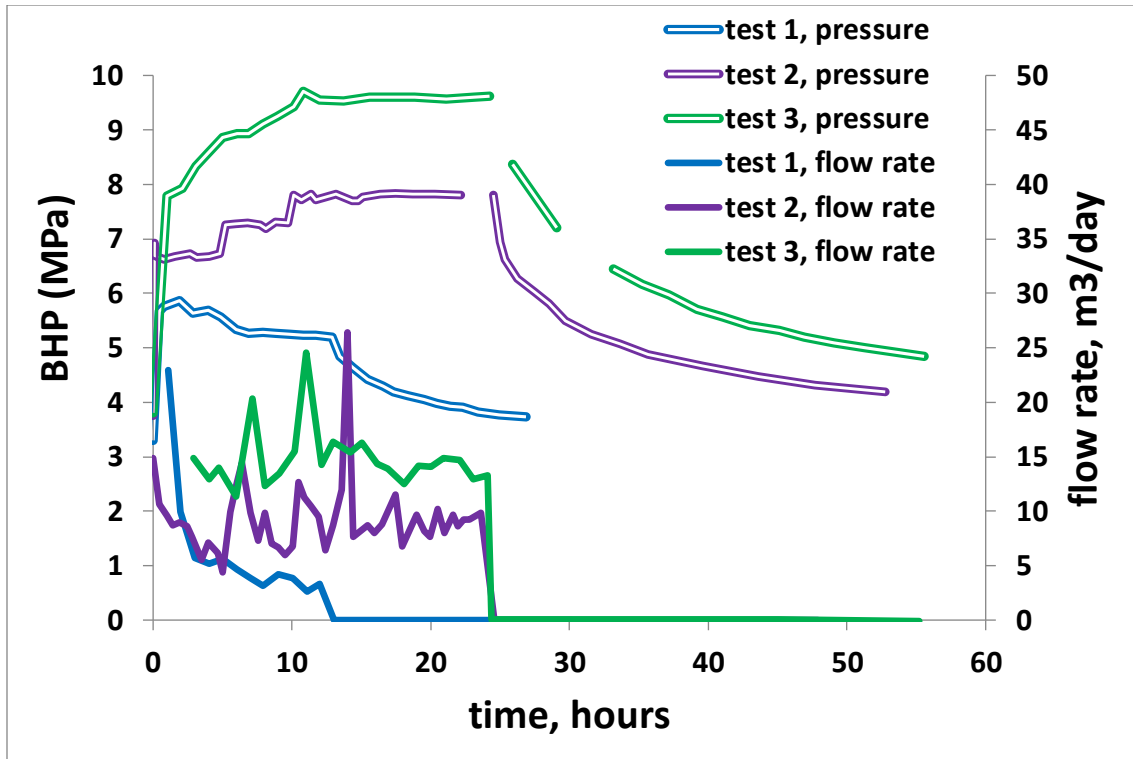


Figure 9: Results of Well Tests in Oil Sands in Burnt Lake Project (Xu, 2010)

5.1 Reservoir Fluid Properties

Different values have been reported for the bitumen viscosity in this field: 40,000 (Yeung and Adamson, 1991; Yeung, 1995), 300,000 cp (Xu, 2010), and more than 80,000 cp (Kisman and Yeung, 1995) at reservoir conditions. Considering such high viscosities, assuming single-phase water flow (immobile bitumen) would be reasonable for a 24-hour test.

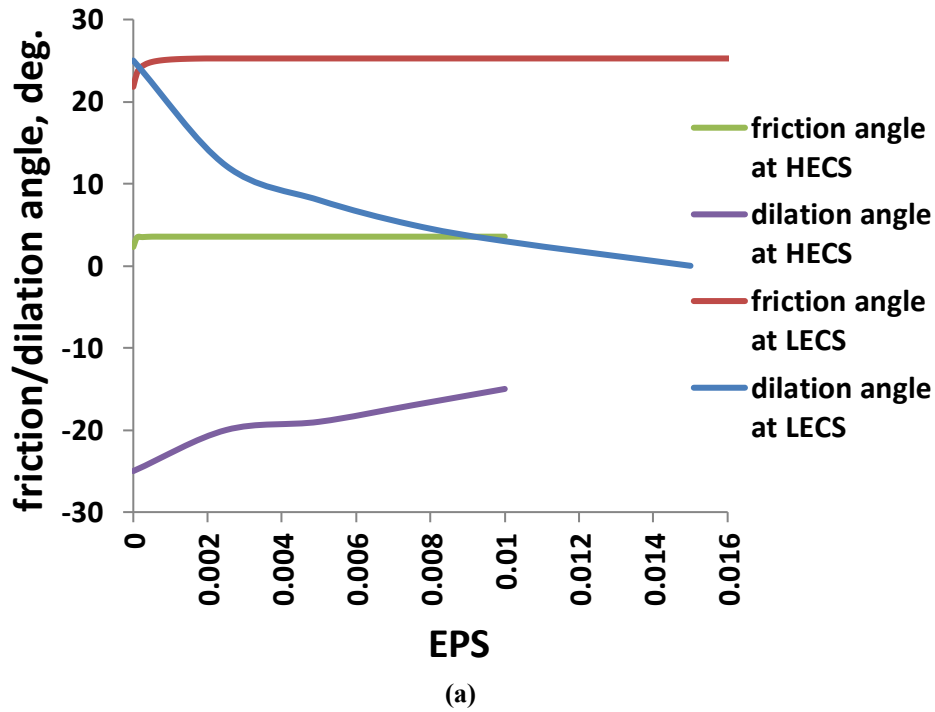
5.2 Oil Sands Properties

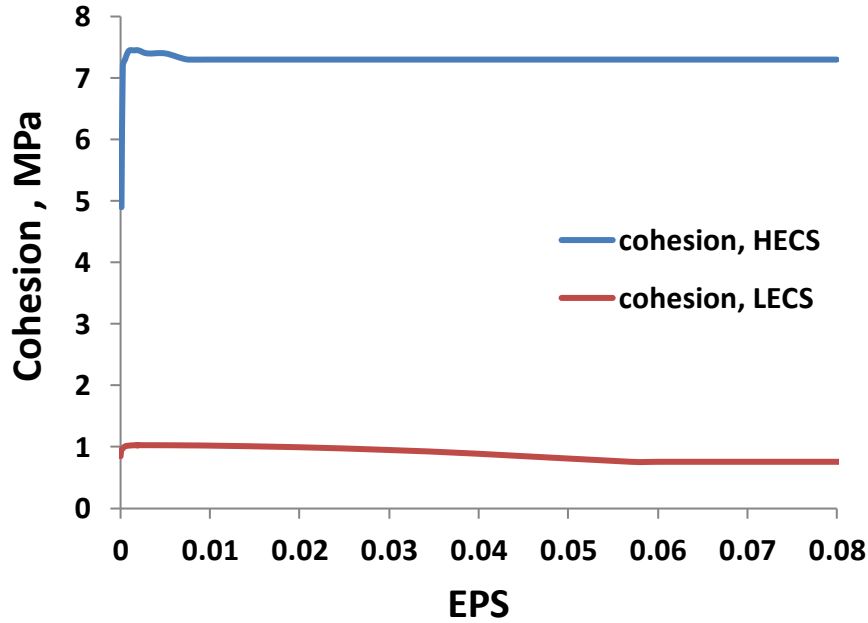
A bilinear Mohr-Coulomb model combined with strain hardening/softening was calibrated against a series of triaxial compression tests on Cold Lake oil sands (Wong et al., 1993). The tests were carried out at temperatures ranging from 20 to 300oC and effective confining stresses ranging from 1 to 18 MPa. The procedure proposed by Nouri et al. (2009) and Jafarpour et al. (2012) was followed to calibrate the constitutive model for the numerical simulations. The average grain size (D50) of the Cold Lake oil sands is 0.08 millimeters (Dusseault, 2001), which is used in fracture energy regularization to reduce mesh dependency of the numerical results.

The calibrated parameters were used in a series of simulations by FLAC2D to verify the numerical match of the stress-strain results with the triaxial testing data. Figure 10a and 10b show the variation of the friction angle, dilation angle and cohesion for Cold Lake oil sands

versus the equivalent plastic strain at both low and high effective confining stress. The results of these simulations are shown in Fig. 11. A typical shear band captured during the simulation at low confining pressure is also shown in this figure.

Plewes (1987) reported the results of Brazilian and unconfined direct tensile tests on cylindrical specimens of rich Athabasca oil sands at a room temperature of 18.5oC. The tensile strength of the rich oil sands was reported to be in the range of 8.1-17.1 kPa, based on the Brazilian tests, and 2.1-6.2 kPa, based on direct tensile test. Plewes (1987) related the apparent tensile strength to the high viscosity of the bitumen at low temperatures and/or negative pore pressure developed during the testing. This tensile strength may be higher at the in-situ temperature of 12 oC. A tensile strength of 100 kPa was assumed in the simulations.





(b)

Figure 10: (a) and (b): Cohesion, Friction and Dilation Angles of Cold Lake Oil Sand Samples as a Function of Equivalent Plastic Strain at Low and High Effective Confining Stresses

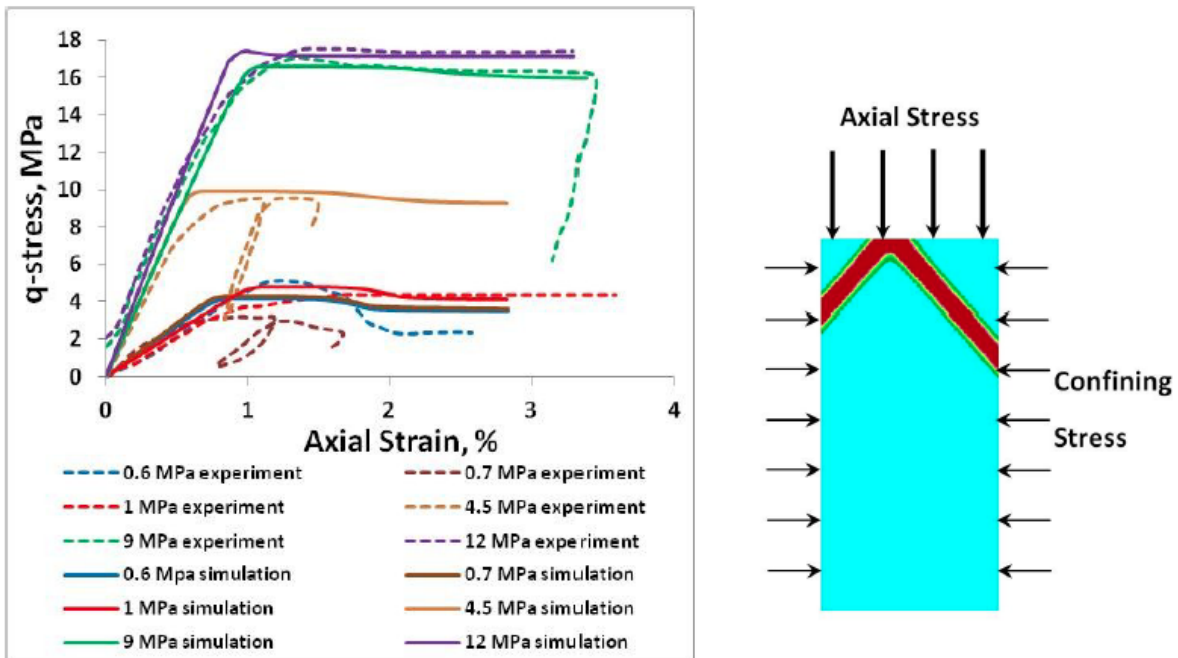


Figure 11: Simulation Results for the Triaxial Compression Tests Performed by Wong et al. (1993). Left: The Stress-Strain Plots for the Entire Test. Right: A Typical Shear Band Captured during the Lowest Effective Stress Test. The Unloading and Loading Cycles are Neglected

5.3 Summary of Oil Sands Properties

Table 4 summarizes the material properties used in the base-case simulation. These properties represent the best estimates based on the limited data in hand.

Table 4: Summary of the Input Material Properties Used in the Numerical Model

Parameter	Value	Parameter	Value
Maximum Principal Stress (MPa) ⁺	10.35	Tensile Strength (MPa) ⁻	0.1
Intermediate Principal Stress (MPa) ⁺	8.28	Initial Cohesion at LECS (MPa) [*]	0.85
Minimum Principal Stress (MPa) ⁺	7.2	Initial Cohesion at HECS (MPa) [*]	4.9
Reservoir Pressure (MPa) ⁺	3.4	Initial Friction Angle at LECS (Degree) ^{**}	21.28
Initial Water Saturation (%) ⁺	30	Initial Friction Angle at HECS (Degree) ^{***}	3.45
Elastic Modulus (MPa) ⁺⁺	Variable	Initial Dilation Angle at LECS (Degree) ^{**}	25
Poisson's Ratio ⁺⁺	Variable	Initial Dilation Angle at HECS (Degree) ^{***}	-24.5
Absolute Permeability (md) ⁻⁻	300	Porosity ⁻⁻⁻	34
B _h and B _H ⁻	2 and 5	Fracture Toughness	1 MPa·√m

⁺ Xu (2010), ⁺⁺ Assessed from laboratory experiments on Cold Lake oil sands performed by Wong et al. (1993), ⁻ From calibrations against experimental data for McMurray oil sands by Touhidi-Baghini (1998), ⁻⁻ Assumed, ⁻⁻⁻ Yeung and Adamson, 1991, ^{*} See Fig. 10b for variations; calculated from laboratory experiments on Cold Lake oil sands performed by Wong et al. (1993), ^{**} At Low Effective Confining Stress (LECS); calculated from triaxial data for Cold Lake oil sands (Clearwater formation) performed by Wong et al. (1993) (see Fig. 10a for variations), ^{***} At High Effective Confining Stress (HECS); calculated from triaxial data for Cold Lake oil sands (Clearwater formation) performed by Wong et al. (1993) (see Fig. 10a for variations)

5.4 Description of Numerical Model

To model the well tests, the bottomhole injection rate was used as a boundary condition. The injection flow rate was adjusted in the model in every time step to match the calculated bottomhole pressure with the measurements in the tests. The calculated flow rate was then compared with the measured values to evaluate the model.

5.4.1 Model and Grid Size

The injection is performed through a vertical wellbore in a 25-m pay for a relatively short duration into a formation with limited permeability to water. Hence, no formation pressurization is expected and the assumption of plane strain would be reasonable. In this case, it is assumed that stresses and strains are uniform along the vertical axis and the strain component in the vertical direction is negligible. For this reason, a 2D plane strain model is considered in the middle of the pay zone and is stretched horizontally perpendicular to the well. Only half of the reservoir is simulated in the model due to symmetry.

The model consists of a wellbore in a 500-meter by 250-meter half-symmetry geometry as shown in Fig. 12. The grid for the plane strain geomechanical model consists of a uniform 1×1-

m2 grid in the area around the injection point with gradually coarser mesh closer to the far field boundaries.

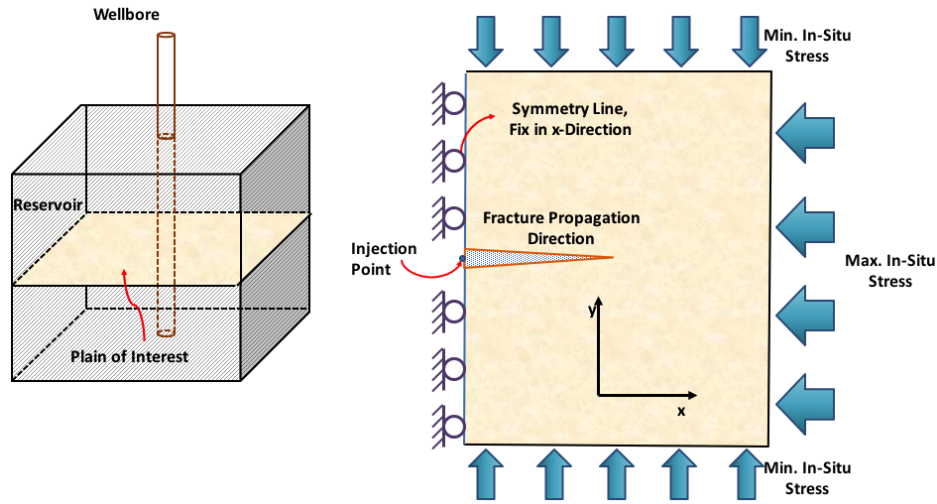


Figure 12: Geometry and Boundary Condition of the Model

5.4.2 Initial and Boundary Conditions

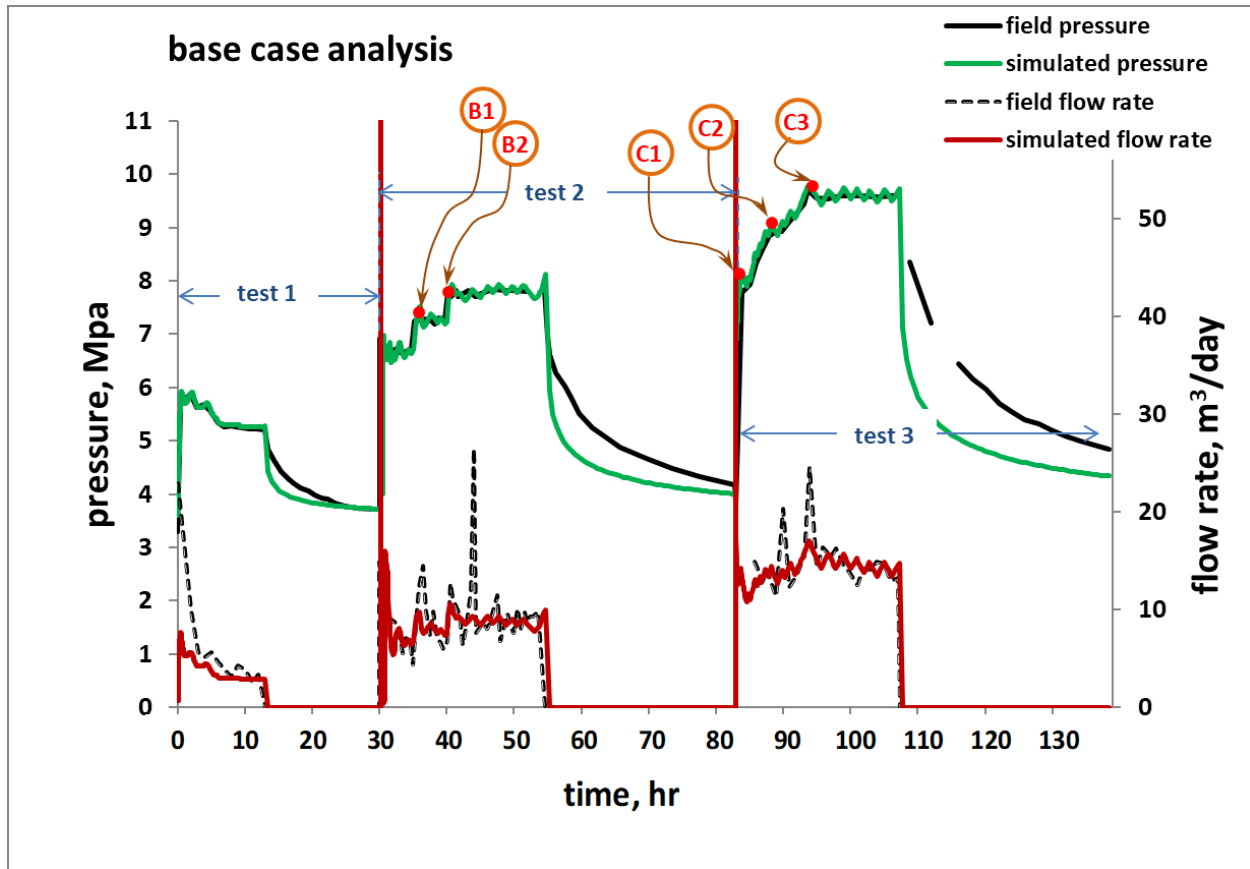
For the geomechanical model, the normal displacements were fixed along the symmetry line. Maximum horizontal stress was applied on the right boundary, and minimum horizontal stress was applied on the top and bottom boundaries of the model as shown in Fig. 12. The maximum (σ_v), intermediate (σ_H) and minimum (σ_h) in situ stresses were 10.35, 8.28 and 7.2 MPa, respectively, and the initial reservoir pressure was 3.3 MPa.

For the flow model, the injection rate was applied from the middle of the left boundary (the symmetry axis). The left boundary, except for the injection point, was considered as a no-flow boundary, and all other boundaries were constant pressure boundaries with pressure equal to the initial reservoir pressure.

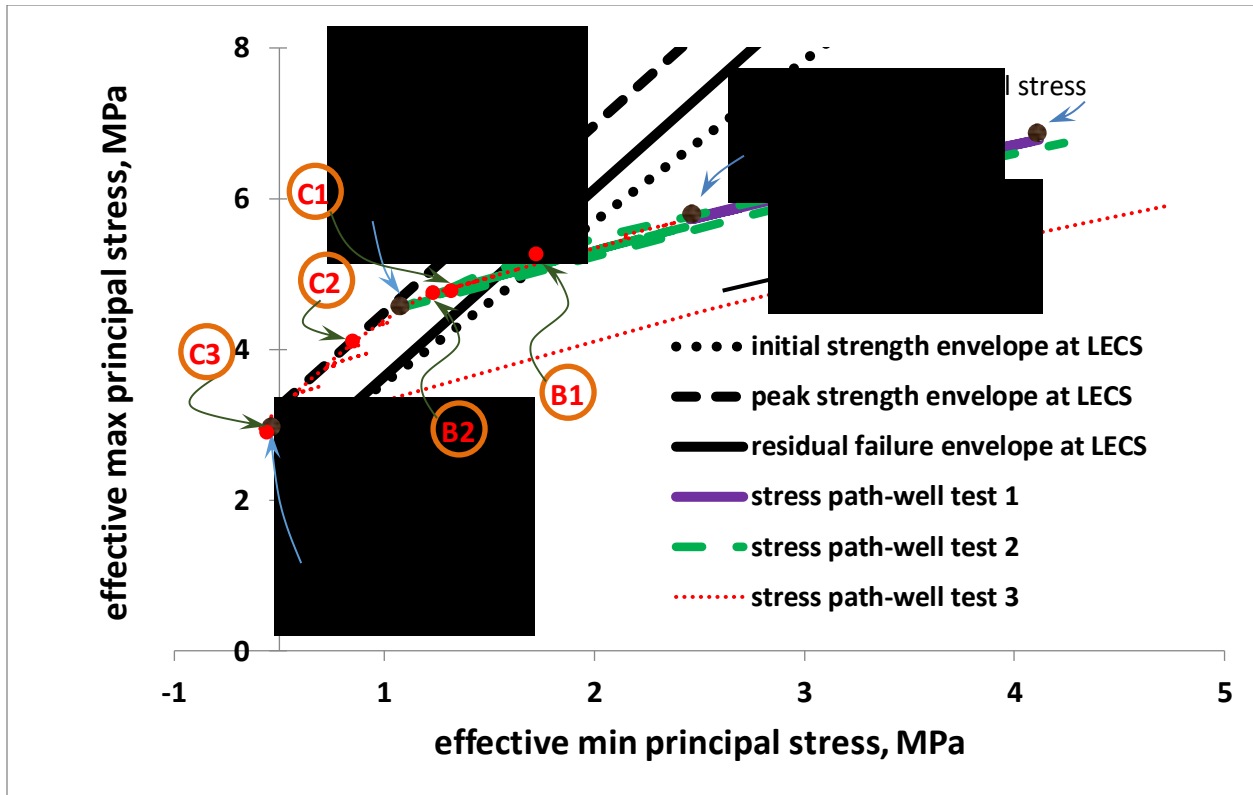
5.4.3 Numerical Model Results

This section compares the simulation results with the measurements from the well tests. The simulation results of the described model are shown in Fig. 13a. As will be discussed later in this section, the numerical results do not indicate any tensile hydraulic fractures during the three well tests. Xu (2010) reported similar findings in his 3D numerical simulations of the same well tests using a strain-induced anisotropic shear permeability model (Wong, 2003). Xu (2010) showed that all the deformations during the well tests were either elastic (in Test 1) or shear

dilative (in Tests 2 and 3). Similarly, in this research, it was found that a hydraulically induced dilated zone formed in the oil sands in Well Tests 2 and 3.



(a)



(b)
 Figure 13: (a) Simulation Results; (b) Stress Path at the Wellbore in the Simulated Well Tests

Figure 13b shows the stress path of the wellbore element in the model. The stress path in Well Test 1 does not intersect the shear failure envelope. It indicates that due to low injection pressures in Well Test 1, the reservoir response is predominantly elastic, similar to the results obtained by Xu (2010). After the shut-in, effective stresses bounce back and the stress path returns to the original stress state.

As confirmed by the stress path, the drop in the bottomhole pressure (BHP) at the early stages of Well Test 1 (Fig. 13a) is caused by the reduced injection rate, not by the development of a hydraulic fracture (either shear or tensile). In late stages of injection in Test 1 (Fig. 13a), the flow rate is nearly constant, resulting in a constant bottomhole pressure.

As per Fig. 13a, a continued increase in the bottomhole pressure in Well Test 2 causes the stress path to intersect with the initial yield envelope at Point B1 at an injection pressure of 7.5 MPa and further advancement of the stress path beyond the initial yield envelope to Point B2 at a pressure of 7.9 MPa. However, the stress path does not reach the peak-strength envelope (see Fig. 13b). The material is still in the strain-hardening stage during Test 2. After shut-in, the stresses bounce back elastically in a path close to the injection path. No tensile fracturing is

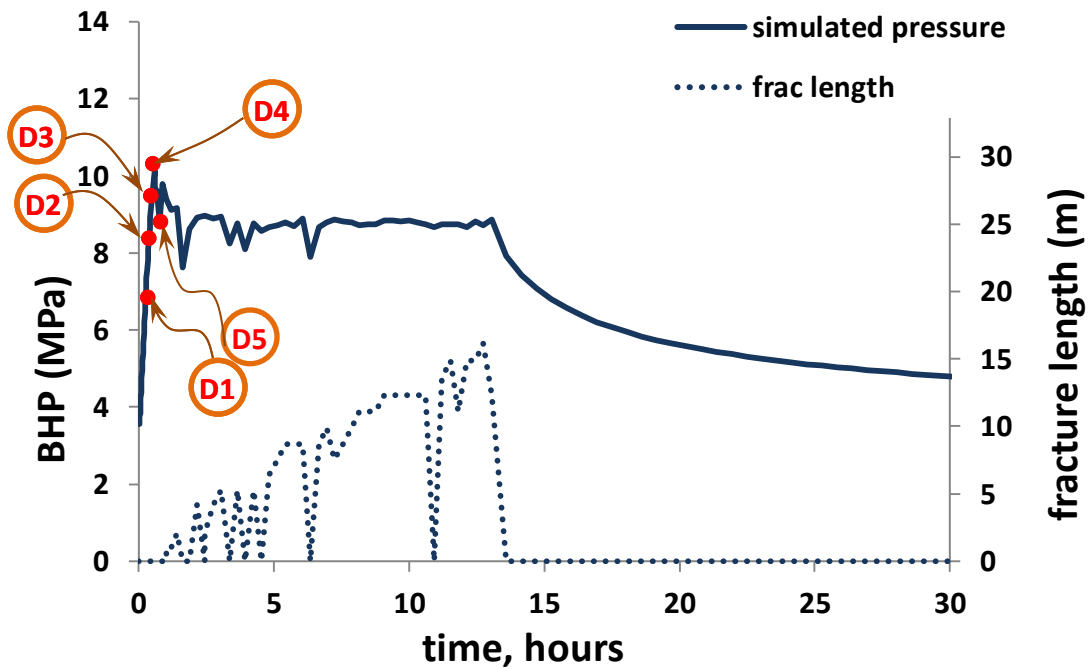
detected numerically during this test. This is consistent with the numerical results reported by Xu (2010).

In Well Pest 3, pressure quickly reaches point C1 (8.1 MPa pressure). The stress path approaches the peak strength at the pressure of 9.0 MPa, shown by Point C2 in Fig. 13b. The stress path then moves on to the peak shear envelope towards Point C3 (9.75 MPa pressure), the highest pressure experienced in this set of well tests. Maintaining the pressure at 9.75 MPa does not result in a tensile fracture, nor further shearing. The oil sand does not show strain softening in Well Test 3 as the stress path stays at the peak strength until the injection is shut in. After the shut-in, the material experiences stress rebound in a path nearly parallel to the path during the injection. The paths do not match due to the plastic deformation. Simulations indicate no tensile fracturing in Test 3 despite the development of a shear yield zone. Xu (2010) reported similar numerical results.

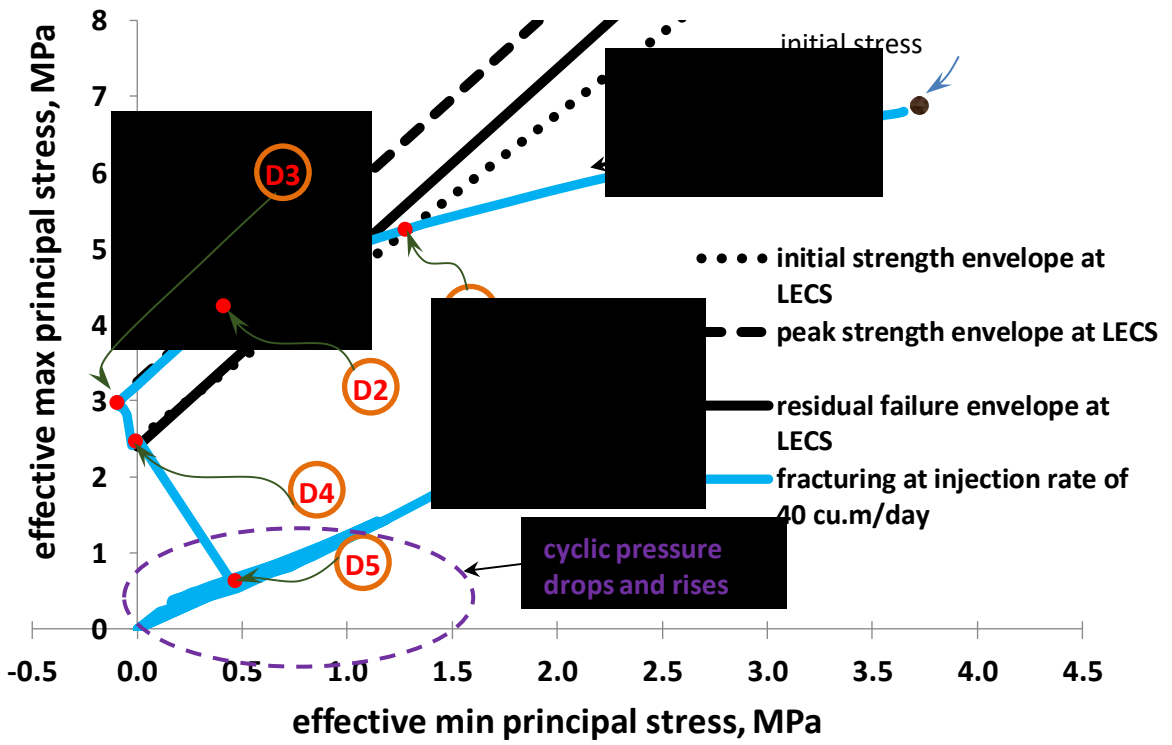
The simulation results indicate no tensile fracture in any of the three well tests, despite the bottomhole pressure of 9.75 MPa in Well Test 3, which is larger than the two initial horizontal stresses (7.2 MPa and 8.28 MPa) but lower than the vertical stress (10.35 MPa).

5.4.4 Fracture Initiation and Propagation Pressure

The simulations so far indicated that no tensile hydraulic fractures developed during the well tests. To investigate the initiation and propagation of a tensile fracture in the reservoir, a hydraulic fracture simulation was carried out using a higher flow rate of 40 m³/day for a duration of 13 hours. The results in the form of bottomhole pressure and fracture length are plotted in Fig. 14a. The figure shows several cycles of fracture closure and reopening during the injection period. The figure also indicates a breakdown pressure of 10.1 MPa, which is close to the maximum in situ stress (i.e., the vertical stress). The propagation pressure is approximately equal to 8.8 MPa, resulting in a 16-meter fracture for a 13-hour injection period.



(a)



(b)

Figure 14: (a) The Fracturing Response of the Oil Sands upon Cold Water Injection; (b) Stress Path at the Wellbore in the Simulated Hydraulic Fracturing

The stress path of the hydraulic fracture simulation in Fig. 14b indicates that shear yielding starts at Point D1 which corresponds to the pressure of 6.76 MPa. Point D2 in Fig. 14b corresponds to the peak shear strength envelope which occurs at a pressure of 8.4 MPa. The compressive stress then drops as the injection pressure continues to rise until the effective stress reaches the tensile strength of the material at Point D3 at 9.4 MPa pressure. A further increase of the bottomhole pressure up to 10.1 MPa (points D3 to D4) degrades the tensile strength of the sand until the tensile strength of the material drops to zero at Point D4 (at 10.1 MPa BHP) when tensile fracturing occurs. The opening of the fracture results in a temporary reduction in pore pressure down to 8.8 MPa at Point D5. At Point D5, the oil sands have totally lost their cohesive and tensile strength due to fracturing. Continuing injection leads to higher pore pressures, reopening the fracture and causing it to propagate. The stress path in Fig. 14b shows that cyclic pressure drops and rises during the injection period. It should be noted that part of these cycles, especially during fracture initiation, can be attributed to mesh size, and may be a numerical artifact.

Figure 15 compares the shear zones of the model for the well tests as well as the model with an artificially higher flow rate (to induce a tensile hydraulic fracture). The shear zone in the high-rate model is much larger than that in the simulated well test, which can be attributed to the higher pore pressures, lower effective stresses and, thus, the lower shear strength. The width of the sheared zone perpendicular to the fracture propagation direction is almost unchanged along the fracture and is approximately equal to 10 meters. It is important to note that the shear zone moves 11 meters ahead of the tensile fracture when the tensile fracture is 16 meters.

Some field observations (in terms of fracture pattern) agree with the results obtained in this research. Microseismic monitoring during fracturing pressure of 79 to 83 MPa in Bossier tight sandstone indicated a half-fracture length of 350-450 feet (Settari et al., 2002a). Settari et al., 2002a believed that the fracture should be shorter than what the microseismic events indicated and also that the microseismic data were related to both the fracture length and the size of the leak-off zone. The microseismic events around the fracture could extend 50 feet ahead of the fracture tip (the fracture length was predicted using standard methods) (Settari et al., 2002b) and also 50 meters sideways (Settari et al., 2002a; Settari et al., 2002b). At early injection time, the microseismic events were focused on the close perimeter of the fracture while later they were found everywhere from the wellbore to the fracture tip (Settari et al., 2002b). Shearing creates a

zone of shear failure/fracture in the proximity of the main tensile fracture. This type of observation has also been reported in laboratory experiments (McElfresh et al., 2002).

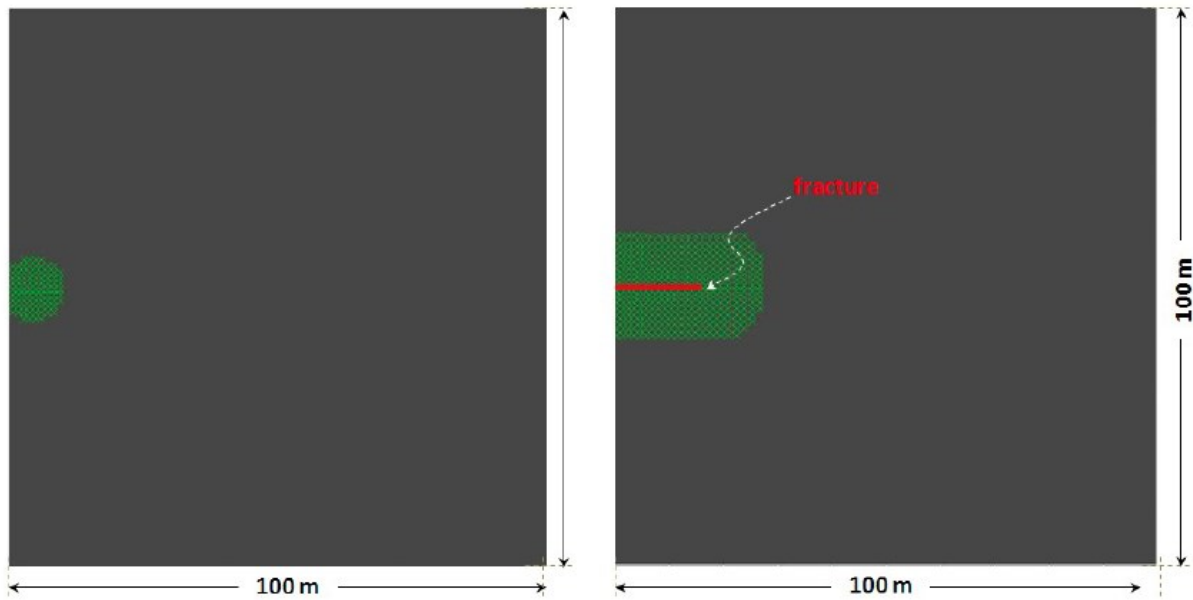


Figure 15: Sheared Yield Zone due to Injection. Left: The Simulated Well Tests. Right: The Induced Hydraulic Fracture Model

6. Conclusion

A partially decoupled hydraulic fracture simulation was described in this study in which the fracture was represented by enhancing the permeability in the reservoir grids. The smeared fracture approach was adopted to simulate tensile fractures and shear failure in the oil sands. Major features of this model include modeling poroelasticity and plasticity, matrix flow, shear failure and tensile fracturing with concomitant permeability enhancement (Touhidi-Baghini's shear permeability and the cubic law, respectively), saturation-dependent permeability, stress-dependent stiffness and gradual degradation of oil sands due to dilatant shear deformation. Such a detailed modelling approach can represent stimulation as well as damage in the formation and can bring the realism of hydraulic fracturing to a new level. Geomechanical effects on fracture initiation and propagation was also included in our modeling through utilizing FLAC2D. Formation displacements rigorously calculated in the geomechanics module, were utilized to give the fracture width while fracture length was calculated based on effective stresses. This can demonstrate the importance of stress change in controlling fluid flow inside the fracture. The modular coupling between fluid flow and geomechanics simulators was carried out through flow properties, i.e. pressure-dependent permeability and porosity. The extremely flexible modular

structure of the system can adapt any advanced commercial geomechanics or reservoir simulator.

Gridding strategy is very important in obtaining more precise dimension of the fracture. Locally refined mesh shows accurate results and, at the same time, does not increase the run time significantly.

The smeared hydraulic fracture model developed in this research was used to simulate three well tests in a cold oil sands reservoir. The model could properly initiate and propagate a hydraulic fracture without having to predefine the fracture direction or location. Simulation results indicate that no tensile hydraulic fracturing formed during the well tests. To investigate the initiation and propagation of a tensile fracture in the reservoir, a hydraulic fracture simulation was carried out using a higher flow rate. Results indicated that the saturation-dependent relative permeability and the permeability alteration due to shear dilation governed the injection response of the oil sands. The saturation-dependent relative permeability influenced the injectivity during the elastic deformation of the oil sands. After shearing, however, the shear dilation of the oil sands, as well as poroelasticity, influenced the injection response.

The work presented in this study was a necessary first step in developing a proppant transport simulator in hydraulic fracturing. We have developed such a numerical tool that integrates reservoir and geomechanics simulator to a proppant transport simulator at the field scale.

7. References

- Behr, A., Mtchedlishvili, G., Friedel, T., & Haefner, F. K. (2006). Consideration of Damaged Zone in a Tight Gas Reservoir Model With a Hydraulically Fractured Well. *SPE Production & Operations*, 21(02), 206-211. doi:10.2118/82298-pa
- Bohloli, B., & de Pater, C. J. (2006). Experimental study on hydraulic fracturing of soft rocks: Influence of fluid rheology and confining stress. *Journal of Petroleum Science and Engineering* 53: 1-12
- Chin, L., Raghavan, R., & Thomas, L. (1998). Fully-Coupled Geomechanics and Fluid-Flow Analysis of Wells with Stress-Dependent Permeability. *Proceedings of SPE International Oil and Gas Conference and Exhibition in China*. doi:10.2523/48857-ms

- Chin, L., & Thomas, L. (1999). Fully Coupled Analysis of Improved Oil Recovery by Reservoir Compaction. SPE Annual Technical Conference and Exhibition. doi:10.2118/56753-ms
- Chin, L. Y. and Montgomery, C. T. 2004. A Numerical Model for Simulating Solid Waste Injection in Soft Rock Reservoirs. SPE Annual Technical Conference and Exhibition, Houston, Texas. 90507
- Cook, B. K., Lee, M. Y., DiGiovanni, A. A., Bronowski, D. R., Perkins, E. D. and Williams, J. R. 2004. Discrete Element Modeling Applied to Laboratory Simulation of Near-Wellbore Mechanics. *International Journal of Geomechanics* 6: 19-27
- Das, B. M. (2013). *Advanced soil mechanics*. 3rd edition. Taylor and Francis, New York.
- Dusseault, M. B. 2001. Comparing Venezuelan and Canadian Heavy Oil and Tar Sands. Canadian International Petroleum Conference, Calgary, AB, Canada. Plewes (1987)
- Ehrl, E., & Schueler, S. (2000). Simulation of a Tight Gas Reservoir with Horizontal Multifractured Wells. SPE European Petroleum Conference. doi:10.2118/65108-ms
- Faisal, A., Dominic, A., Raj, B., & Issaka, M. (2004). Pressure Transient Analysis of Horizontal Wells in a Fractured Reservoir; Gridding Between Art and Science. Proceedings of SPE Asia Pacific Conference on Integrated Modelling for Asset Management. doi:10.2523/87013-ms
- Garon, A., Lin, C., & Dunayevsky, V. (1988). Simulation of Thermally Induced Waterflood Fracturing in Prudhoe Bay. Proceedings of SPE California Regional Meeting. doi:10.2523/17417-ms
- Gil, I. 2005. Hydraulic fracturing of poorly consolidated formations: Considerations on rock properties and failure mechanisms. PhD Thesis. University of Oklahoma, Oklahoma
- Gil, I. and Roegiers, J. 2006. The Effect of Fluid Leakoff on Rock Failure Mechanisms During Frac-Pack Treatments. Page 7 International Symposium and Exhibition on Formation Damage Control. Society of Petroleum Engineers, Lafayette, Louisiana U.S.A. 98170
- Gringarten, A. C., Ramey, H. J., & Raghavan, R. (1974). Unsteady-State Pressure Distributions Created by a Well With a Single Infinite-Conductivity Vertical Fracture. *Society of Petroleum Engineers Journal*, 14(04), 347-360. doi:10.2118/4051-pa
- Gutierrez, M., & Makurat, A. (1997). Coupled HTM modelling of cold water injection in fractured hydrocarbon reservoirs. *International Journal of Rock Mechanics and Mining*

- Sciences & Geomechanics Abstracts,34(3-4), 429-429. doi:10.1016/s0148-9062(97)00033-8
- Hagoort, J., Weatherill, B. D., & Settari, A. (1980). Modeling the Propagation of Waterflood-Induced Hydraulic Fractures. *Society of Petroleum Engineers Journal*,20(04), 293-303. doi:10.2118/7412-pa
- Heffer, K., Koutsabeloulis, N., & Wong, S. (1994). Coupled geomechanical, thermal and fluid flow modelling as an aid to improving waterflood sweep efficiency. *Rock Mechanics in Petroleum Engineering*. doi:10.2118/28082-ms
- Hoek, V. D., Matsuura, T., M., D., & Gheissary, G. (1996). Simulation of produced water re-injection under fracturing conditions. *Proceedings of European Petroleum Conference*. doi:10.2523/36846-ms
- Hustedt, B., Qiu, Y., Zwarts, D., & Hoek, P. J. (2005). Modeling Water-Injection Induced Fractures in Reservoir Simulation. *SPE Annual Technical Conference and Exhibition*. doi:10.2118/95726-ms
- Jafarpour, M., Rahmati, H., Azadbakht, S., Nouri, A., Chan, D., Vaziri, H. (2012) Determination of Mobilized Strength Properties of Degrading Sandstone, Soils and Foundations, 52(4), Aug.
- Ji, L., Settari, A. T., Sullivan, R., & Orr, D. (2004). Methods for modeling dynamic fractures in coupled reservoir and geomechanics simulation. *SPE Annual Technical Conference and Exhibition*. doi:10.2118/90874-ms
- Ji, L., Settari, A., & Sullivan, R. B. (2006). A new approach to hydraulic fracturing modeling - fully coupled with geomechanical and reservoir simulation. *SPE Europec/EAGE Annual Conference and Exhibition*. doi:10.2118/99428-ms
- Ji, L. (2008). Modeling hydraulic fracturing fully coupled with reservoir and geomechanical simulation. ProQuest.
- Ji, L., Settari, A. and Sullivan, R. B. 2009. A Novel Hydraulic Fracturing Model Fully Coupled With Geomechanics and Reservoir Simulation. *SPE Journal* 14: 423-430. SPE-110845-PA
- Kisman, K. E. and Yeung, K. C. 1995. Numerical Study of the SAGD Process in the Burnt Lake Oil Sands Lease. *Society of Petroleum Engineers*. Nouri et al. (2009) and Jafarpour et al. (2012)

- Lebel, J. P. (2002). Dynamic fracture modelling approach for cold lake cyclic steam stimulation. SPE International Thermal Operations and Heavy Oil Symposium and International Horizontal Well Technology Conference. doi:10.2118/79010-ms
- Longuemare, P., Detienne, J., Lemonnier, P., Bouteca, M., & Onaisi, A. (2001). Numerical modeling of fracture propagation induced by water injection/re-injection. SPE European Formation Damage Conference. doi:10.2118/68974-ms
- Marti, J., and Cundall, P.A., 1982. Mixed Discretization Procedure for Accurate Solution of Plasticity Problem, *Int. J. Num. Methods and Anal. Methods in Geomech.*, 6, 129-139.
- McElfresh, P. M., Khodaverdian, M. F. and Baycroft, P. D. 2002. Frac Packing in Soft Formations: Low Efficiency Fluids Exacerbate Formation Damage. Page 12 International Symposium and Exhibition on Formation Damage Control. Society of Petroleum Engineers, Lafayette, Louisiana
- Miranda, C. G., Soliman, M. Y., Settari, A., & Krampol, R. (2010). Linking reservoir simulators with fracture simulators. SPE Eastern Regional Meeting. doi:10.2118/137752-ms
- Nghiem, L., Forsyth, P., & Behie, A. (1984). A fully implicit hydraulic fracture model. *Journal of Petroleum Technology*, 36(07), 1191-1198. doi:10.2118/10506-pa
- Nouri, A., Kuru, E., & Vaziri, H. (2009). Elastoplastic Modelling of Sand Production Using Fracture Energy Regularization Method. *Journal of Canadian Petroleum Technology*, 48(04), 64-71. doi:10.2118/09-04-64
- Papanastasiou, P. 1997a. The influence of plasticity in hydraulic fracturing. *International Journal of Fracture* 84: 61-79
- Papanastasiou, P. C. 1997b. A coupled Elastoplastic Hydraulic Fracturing Model. *International Journal of Rock Mechanics and Mining Sciences* 34: 240.e241-240.e215
- Papanastasiou, P. 1999. An efficient algorithm for propagating fluid-driven fractures. *Computational Mechanics* 24: 258-267
- Roussel, N.P., and Sharma, M.M., 2010. Quantifying Transient Effects in Altered-stress Refracturing of Vertical Wells, SPE 119522-PA, SPE Journal, Vol 15, No. 3, pp. 770-782, September.
- Roussel, N.P., and Sharma, M.M., 2011. Optimizing Fracture Spacing and Sequencing in Horizontal-Well Fracturing, SPE Production & Operations, Vol. 26, No. 2, pp. 173-184, May.

- Settari, A., Kry, P. R. and Yee, C. T. 1989. Coupling Of Fluid Flow And Soil Behaviour To Model Injection Into Uncemented Oil Sands. *The Journal of Canadian Petroleum Technology* 28: 12. 89-01-08
- Settari, A. (1980). Simulation of hydraulic fracturing processes. *Society of Petroleum Engineers Journal*,20(06), 487-500. doi:10.2118/7693-pa
- Settari, A. (1988). Quantitative analysis of factors influencing vertical and lateral fracture growth. *SPE Production Engineering*,3(03), 310-322. doi:10.2118/13862-pa
- Settari, A., Puchyr, P., & Bachman, R. (1990). Partially decoupled modeling of hydraulic fracturing processes. *SPE Production Engineering*,5(01), 37-44. doi:10.2118/16031-pa
- Settari, A., Ito, Y. and Jha, K. N. 1992. Coupling Of A Fracture Mechanics Model And A Thermal Reservoir Simulator For Tar Sands. 92-09-02
- Settari, A., & Mourits, F. M. (1994). Coupling of geomechanics and reservoir simulation models. *Computer Methods and Advances in Geomechanics*, 3, 2151-2158.
- Settari, A., & Mourits, F. (1998). A coupled reservoir and geomechanical simulation system. *SPE Journal*,3(03), 219-226. doi:10.2118/50939-pa
- Settari, A., & Walters, D. A. (2001). Advances in coupled geomechanical and reservoir modeling with applications to reservoir compaction. *SPE Journal*,6(03), 334-342. doi:10.2118/74142-pa
- Settari, A., Sullivan, R. B. and Bachman, R. C. 2002a. The Modeling of the Effect of Water Blockage and Geomechanics in Waterfracs. *SPE Annual Technical Conference and Exhibition*, San Antonio, Texas. 77600
- Settari, A., Sullivan, R. B., Walters, D. A. and Wawrzynek, P. A. 2002b. 3-D Analysis and Prediction of Microseismicity in Fracturing by Coupled Geomechanical Modeling. *SPE Gas Technology Symposium*, Calgary, Alberta, Canada. 75714
- Tortike, W. S., & Ali, S. M. (1993). Reservoir simulation integrated with geomechanics. *Journal of Canadian Petroleum Technology*, 32(05).
- Touhidi-Baghini, A. 1998. Absolute permeability of McMurray Formation oil sands at low confining stresses. PhD Thesis. University of Alberta, Edmonton
- van Dam, D. B., Papanastasiou, P. and Pater, C. J. d. 2000. Impact of Rock Plasticity on Hydraulic Fracture Propagation and Closure. *SPE Annual Technical Conference and Exhibition*. Copyright 2000, Society of Petroleum Engineers Inc., Dallas, Texas. 63172

- Waite, M. E., Ge, S., & Spetzler, H. (1999). A new conceptual model for fluid flow in discrete fractures: an experimental and numerical study. *Journal of Geophysical Research: Solid Earth*, 104(B6), 13049-13059.
- Weill, L., & Latil, M. (1992). Modeling hydraulic fracture in finite difference reservoir simulator. ECMOR III - 3rd European Conference on the Mathematics of Oil Recovery. doi:10.3997/2214-4609.201411092
- White, F. M. 2011. Fluid Mechanics. McGraw Hill
- Wong, R. C. (2003). A model for strain-induced permeability anisotropy in deformable granular media. *Canadian geotechnical journal*, 40(1), 95-106.
- Wu, R. 2006. Some Fundamental Mechanisms of Hydraulic Fracturing. Georgia Institute of Technology, Atlanta
- Xu, B. 2010. Finite element simulation of hydraulic fracturing in unconsolidated sands. Ph.D. Dissertation. University of Calgary, Calgary, AB
- Xu, B. and Wong, R. C. K. 2010. A 3D Finite Element Model for History Matching Hydraulic Fracturing in Unconsolidated Sands Formation. *Journal of Canadian Petroleum Technology* 49: 58-66
- Xu, B., Yuan, Y. and Wong, R. C. K. 2010. Modeling of the Hydraulic Fractures In Unconsolidated Oil Sands Reservoir. 44th U.S. Rock Mechanics Symposium and 5th U.S.-Canada Rock Mechanics Symposium. American Rock Mechanics Association, Salt Lake City, Utah. 10-123
- Yeung, K. C. and Adamson, M. F. 1991. Burnt Lake Project - Bitumen production form the Cold Lake oil sands deposit without steam. Pages 77-83 44th Canadian Geotechnical Conference. Canadian Geotechnical Society, Calgary, AB, Canada
- Yeung, K. C. 1995. Cold Flow Production of Crude Bitumen at the Burnt Lake Project, Northeastern Alberta. Sixth UNITAR International Conference on Heavy Crude and Tar Sands, Houston, Texas
- Yuan, S. C., & Harrison, J. P. (2005). Development of a hydro-mechanical local degradation approach and its application to modelling fluid flow during progressive fracturing of heterogeneous rocks. *International Journal of Rock Mechanics and Mining Sciences*, 42(7-8), 961-984.

- Zhai, Z. and Sharma, M. M. 2005. A New Approach to Modeling Hydraulic Fractures in Unconsolidated Sands. SPE Annual Technical Conference and Exhibition. Society of Petroleum Engineers, Dallas, Texas. SPE 96246
- Zhai, Z. 2006. Fracturing and Fracture Reorientation in Unconsolidated Sands and Sandstones. PhD Thesis. The University of Texas at Austin, Austin.
- Zimmerman, R. W., & Bodvarsson, G. S. (1996). Hydraulic conductivity of rock fractures. *Transport in porous media*, 23(1), 1-30.

Appendix A: Geomechanical Module, FLAC 2D

Fast Lagrangian Analysis of Continua (FLAC) is a 2D explicit finite different program, developed by ITASCA Consulting Group Inc. ITASCA has developed several geomechanical/geotechnical software including FLAC2D/FLAC 3D, Universal Distinct Element Code (UDECODE/3DECODE), and Particle Flow Code (PFC).

FLAC is a 2D program, however, 3D problems could be solved using axisymmetric and plane strain concepts. FLAC 3D was also developed to address the 3D problems, which were not follow the axisymmetric and plane strain condition.

In FLAC, the material is represented by complex grids and groups. Grids could be easily adjusted/designed by the user to represent the geometry of the problem. The studied material could yield and flow during the simulation. Moreover, the assigned grid could deform in case of the large-strain mode and move with the material. The mixed-discretization zoning technique (Marti and Cundall, 1982) and explicit, Lagrangian calculation scheme, assure the accurate modeling of the plastic flow.

FLAC could be coupled with other software such as MATLAB, as input and outputs of the software could be managed by built-in programming language (FISH). The command-driven option of FLAC enables this program to be controlled by external platforms such as MATLAB.

The software considers different constitutive models to simulate the elastic, plastic and post plastic behavior of the geomaterial. Moreover, the built-in FISH enables the users to develop the customized constitutive model.

Constitutive models control the linear/nonlinear behavior of each element under applied forces. Built-in constitutive models could model variety of behaviors including: hardening and softening, presence of ubiquitous joints, swelling, anisotropic elasticity, and viscoplastic creep

model. These constitutive models also cover different failure criteria for geomaterials such as Drucker-Prager, Mohr-Coulomb, von Mises, and Hoek- Brown.

FLAC was originally intended to study the behavior of the structures mainly in soil and rock, under elastic and/or plastic conditions. It was originally designed for geotechnics and mining application, however, overtime, it has been used for variety of applications. Since its introduction in 1986 by Peter Cundall, FLAC has been widely used in geomechanical, and geotechnical projects in petroleum engineering, mining, and rock engineering.

FLAC has been also used in modeling the fractures (Roussel and Sharma, 2010; 2011). Roussel and Sharma (2010; 2011) performed a numerical investigation using FLAC3D with a coupled finite difference approach. The main objective of the investigation was to understand the effect of fracture development on stress reorientation and the stress state around the fractures.

In current study, FLAC was used as the geomechanical module. MATLAB was employed to code our in-house developed fluid flow simulator. It was also employed to couple the FLAC and the fluid flow simulator.